Characterization of the angular and temporal response for an event-based asynchronous sun sensor

Ivar Kjellesvig Egeland

Thesis submitted for the degree of
Master in Electronics: Microelectronics and
Sensor technology
60 credits

Institute for Physics
Faculty of mathematics and natural sciences

UNIVERSITY OF OSLO

Spring 2023

Characterization of the angular and temporal response for an event-based asynchronous sun sensor

Ivar Kjellesvig Egeland

Characterization of the angular and temporal response for an event-based asynchronous sun sensor

http://www.duo.uio.no/

Printed: Reprosentralen, University of Oslo

Abstract

Traditional sun sensors work by measuring accumulated charge in pixels over a fixed time period, while event based sun sensors work by the pixels triggering an interrupt signal when they have accumulated enough charge. These pixels send their address on an asynchronous data bus. The pixel event latency is based on the pixel illumination, where higher illumination means more energy which results in shorter triggering latency. Thus, temporal data in the form of pixel event latency can be used to derive illumination.

In this work, an event based sun sensors angular and temporal data is characterized in an attempt to investigate use cases for the temporal data. A readout system is designed and presented in this thesis. The readout system contains both the asynchronous sun sensor, as well as a traditional sun sensor used as a calibrated reference. The angular and temporal data is characterized in a set of tests using a high power LED lamp with the read out system mounted on a spinning rate table.

The measured pixel delay formed a pattern of triangle waves which exhibited a linear behavior. The readout system was able to measure the changes in the temporal data at 0.1° changes in the angle of incidence, while the sun sensor's angular data provides a worst case resolution at 1.88° degrees.

The first effort to use the temporal data for angular correction failed due to the instability of the angular data in the measurements performed. Improvements to the readout system and data processing, as well as the event based sun sensor, is proposed.

Acknowledgments

No major undertaking is ever truly taken alone, and thus acknowledgments are the bare minimum reward that can be given. I am deeply grateful for all parties and institutions involved in helping, guiding, proofreading and supporting me through this work.

A special thanks goes to Ketil Røed as the primary supervisor for this project. Without Lukazs Farian's sensor, there would be no basis for this work. Espen Trondsen deserves an apology for having his lab constantly raided for equipment. Tore André Bekkeng will get credit as co-supervisor, and I am grateful for the mentoring you have given over the years.

This major undertaking could truly not have been accomplished without the unwavering help, love and support from a loved one. This could simply not be possible without you and all the help you have given. I can therefore safely conclude that I am the luckiest man alive to have you, Carina, in my life.

March, 2023

Ivar Kjellesvig Egeland

Contents

List of Tables

List of Figures

1 Introduction

In recent years, there has been a drive to decrease the cost, complexity and development time of space missions - to make space more accessible. This trend has been dubbed *New Space*. One major aspect of New Space is to try to find Commercial off the Shelf components not intended specifically for aerospace, but which could be used on a low cost satellite. Some adaptions and qualification testing is, of course, necessary, but the result is often a small and cheap satellite that is fully functional, but with a shorter life expectancy compared to traditional *Old Space* satellites. While a *fail fast* approach is generally accepted in the New Space philosophy, the attitude determination and control system are vital for all missions and therefore a large industry has evolved around making attitude determination sensors for New Space satellites.

Sun sensors have been used extensively in attitude determination and control systems for both sounding rockets and satellites, due to their simple working principle. State of the art New Space sun sensors can be small and cheap, as they use few resources to operate and are reasonably accurate. Sun sensors also exist on the opposite side of this scale; large, expensive models that require both a more substantial amount of power and processing to operate, but that have a better accuracy, and that can operate in a larger part of an orbit. The question then becomes: Can the simple sun sensor design be improved? What are the major drawbacks? And, most important to this work, can a new approach to the sun sensor design find its use in aerospace on low cost satellites, and how does it compare to typical New Space sun sensors?

This work relies on the sensor concept introduced by Dr. Lukasz Farian in his PhD thesis [4]. To try to answer the questions mentioned in the previous paragraph, this work proposes data processing Farian's sensor to try to increase the resolution and accuracy. To this end a readout system is designed, and Farian's sensor is characterized. During the course of this work, a launch opportunity on a student satellite was introduced with the possibility to test the sensor in situ. Hence, the readout system is designed to support both the characterization process in a controlled lab, as well as be able to produce relevant performance measurements when employed on a small 1U Cubesat. Thus, this work will include topics on sun sensors in general, the theory behind Farian's sensor, its characterization and calibration, as well as techniques to rapidly make use of a flight opportunity, and constraints related to use in space.

1.1 Background

In his thesis [4], Farian has made an event based sun sensor. In short, the sun sensor differs from traditional sensors in that it has multiple individual pixels, which, after being exposed to enough photons, send out an interrupt signal, where the only information is the pixel address. Traditional sensors, however, typically read out all pixels at the same time at a fixed rate. Due to the asynchronous nature of Farian's sensor, it is able to achieve a very high temporal resolution, which in turn is a function of the intensity and angle of incidence of the light, while traditional sensors are constrained by set exposure times.

Farian proposes that the sun sensor should be specifically suitable for use on sounding rockets and satellites. This suggestion is based on performance specifications with other state of the art sun sensors, but does not delve deeper to consider the use cases or constraints found in aerospace. Also, while the low power consumption, wide field of view, and good accuracy is desirable in all sensors used in space systems, these parameters alone are not enough to fully evaluate how well it will perform in space.

The sun sensor is an interesting sensor with a high potential for use on different applications, but because of this, it may be at a high risk of various inaccuracies. In this work, some of these errors are discussed, but the main focus is on using an un-traditional sensor in an unconventional way in the search of ways to improve the sensor concept by specifically looking into the asynchronous nature, and the resulting temporal data for potentially better accuracy.

1.2 Motivation and method

The primary goals of this work are to evaluate an experimental, novel sensor [4] for use as an alternative type of sun sensor, develop signal processing techniques for the sensor, and define a series of tests used to characterize said sensor.Thus, the method used in this work is to gather an understanding of the test subject, in this case the sun sensor, followed by some modeling of the sensor behavior. Then the design of an embedded system capable of measuring the desired effects and modeled behavior is performed, before the experiments can begin.

This will both be used in lab measurements, and as an actual payload for in situ testing on a student satellite. The readout system will consist of the electronics needed to control, read and process data from the sun sensor. The readout system will also contain a commercial sun sensor made for low cost satellites as a reference sensor. The reason for this is to be able to make the best "apples to apples" comparison, having two different types of sun sensors receiving the same input. If the new sensor can deliver performance greater, or require less computing resources from a system than a traditional based sensor, then the sensor concept should be considered a success. By both employing lab characterization and in situ measurements, the technology readiness level would rapidly rise, and hopefully surface previously unknown use cases and potential constraints.

This work is entered into with the philosophy that a novel sensor should open avenues for new and related novel concepts. The novel sensor concept provides temporal data as well as angular data. This work proposes that this data could be leveraged if it could be proved that the temporal data has a consistent response.

Due to the nature of novel work, few sources other than the primary genesis source for the sensor exist. Good user guides are replaced by academic findings, which in turn risks increasing the work load of getting a system up and running, as well as creating difficulty in using the sensor as intended.

1.3 Goals

In short the goals can be summarized as bullet lines:

- Characterize the angular and temporal performance of the sensor within the stated field of view.
- Investigate if the temporal data can be used to improve the sensors accuracy.
- Evaluate if the current sensor design is mature for use in space.
- Make a system that provides the means to perform in situ test of the sensor on a student satellite.

1.4 Outline of the thesis

This work consists of 13 chapters, which in turn fall into three parts; Part 1 (sections 1-3) provides the background information and theory needed; Part 2 (sections 4-8) describes the design work performed; Part 3 (sections 9-13) presents the tests performed and their corresponding results, while also containing the discussion and conclusion for the work.

- Section 1 gives a brief introduction on the background and motivation for this work
- Section 2 gives an overview of the theory and concepts used by the sensor system

- Section 3 contains the different models and equation used to describe the sensor's working principle
- Section 4 gives an explanation of the readout system design
- Section 5 describes the electrical design
- Section 6 describes the FPGA design
- Section 7 contains the software design
- Section 8 is a short section showing the mechanical enclosure
- Section 9 lists the different lab tests performed
- Section 10 gives some insight into the in situ tests on a planned student satellite
- Section 11 shows the results from the tests performed
- Section 12 is a discussion chapter
- Section 13 is a short summary and the work's conclusion

2 Theory

2.1 Chapter outline and introduction

This chapter gives the background theory needed to explain the inner workings for the event based sun sensor, as well as some related topics meant to provide further context to the sensor's usage. This chapter does not include any theory related to embedded systems, nor non-imaging sensor electronics. A general understanding of the photo-electric effect, as well as electronics and embedded systems, is assumed. No prior knowledge of space systems, best practices or constraints are required, and relevant information and theory will be provided in this chapter.

First some theory on light is presented, followed by a brief overview on basic imaging sensors. Thereafter, the working principles of analog and digital sun sensors are introduced. Lastly, the relevant inner workings of the event based sun sensor are presented in depth.

2.2 A light overview on light

As light is what sun sensors require to work, an *light* overview on light and the effects relevant for sun sensors is presented in this section.

Visible light is a portion of the electromagnetic wave spectrum which stretches from around 380 nm to 770 nm [10]. Visible light can behave, and be modeled as, waves, but also particles. These particles are referred to as *photons*. At shorter wavelengths than visible light we have the ultra violet band, at 100 nm to 400 nm. At longer wavelengths we find the infrared band, from 770 nm all the way up to 1 mm. For this work, the visible light and the near infrared band are of most interest, as these wavelengths are able to interact with silicon based semiconductors.

Silicon photodiodes are generally more sensitive to photons with a wavelength at the red end, i.e. longer wavelength, of the electromagnetic wave spectrum, than the blue end [10]. This is in spite of the fact that the shorter wavelengths contain more energy, as seen in figure 1 and in equation (1), where Q is the photon energy, h is Planck's constant, c is the speed of light, and λ is the wavelength of the photon.

$$Q = \frac{hc}{\lambda} \tag{1}$$

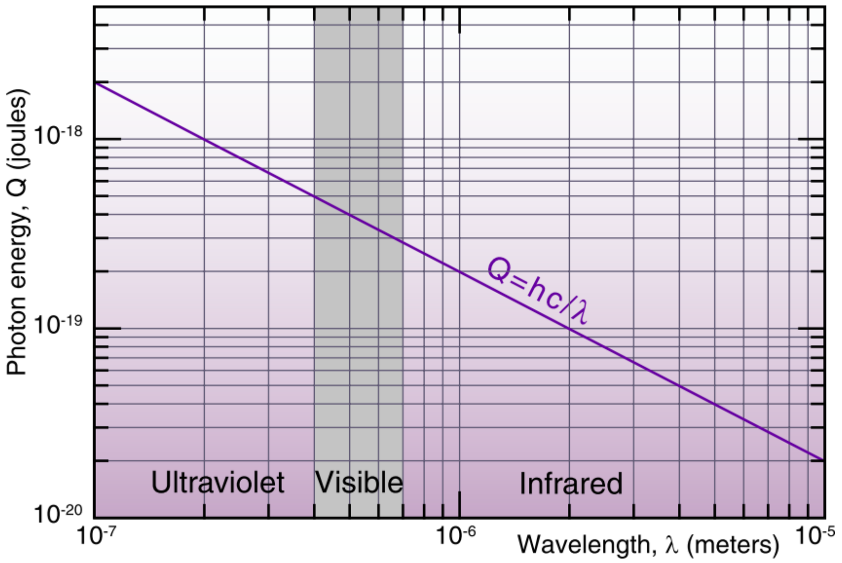

Figure 1: Photon energy in joules vs wavelength, taken from [10].

2.2.1 Cosine law

Lambert's cosine law shows the relationship between the angle of incidence on a surface and reflected/absorbed illumination of light. The absorption rate is on its highest when the light source is normal to the surface in question, and falls with the cosine of the angle of the incidence. We can write the cosine law in a simplified form as

$$E_\theta = E_{\max} \cos\theta \tag{2}$$

when the light source can be treated as an illumination flux instead of a single point of illumination, which is dependent on the distance between source and surface. Equation (2) shows that the illumination at a given angle is directly proportionate to the cosine of the angle. Here $E(\theta)$ is used to denote illumination at a given angle θ, and $E_{\max}$ is the maximal illumination. Figure 2 shows the cosine law in effect.

The material and roughness of the surface dictates the applicability of cosine law. Surfaces that have an ideal diffuse reflection are considered to be a lambertian surface. Silicon semiconductors' random, non uniform surfaces are considered to be a somewhat Lambertian surface, making the cosine law applicable for sun sensors.

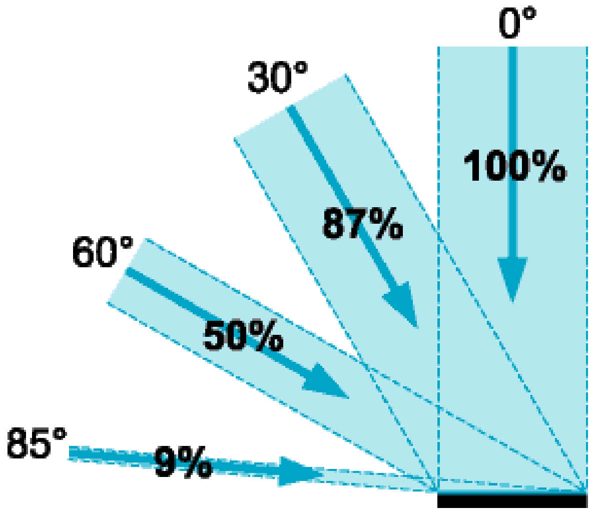

Figure 2: Illustrated effective illumination due to the cosine law in equation (2). Taken from [10].

2.2.2 Extraterrestrial sunlight

This subsection provides some insight into what is relevant for all sun sensors, namely extraterrestrial sunlight.

The spectra of sun light can be modeled as black body radiation, with a temperature of 5770 K. As seen in figure 3, the peak of the wavelength flux is around 500 nm. The curve falls sharply on shorter wavelengths, and a bit slower on the longer wavelengths. The bulk of the spectral density is located in the region of visible light, and the region where silicon semiconductors are able to be affected.

The average distance between the Earth and the Sun is 1 au (Astronomical unit), or 150×10^6 km. Due to large distance, objects in different orbits around the Earth can be considered to have the same distance to the Sun. The incoming light from the Sun is simplified to be considered parallel for all practical purposes due to the large distance to the Earth, even if the light has a 0.5° view angle.

At 1 au, the irradiance of the sun, dubbed the *solar constant*, is measured to be $1360.8\,\mathrm{W\,m^{-2}}$ at the minimum of a cycle [7]. The term *constant* is a bit misplaced, as the activity, and thus the output, of the sun varies in an 11 year cycle. The solar constant is used to estimate the expected incoming light, and thus the current generated by the photodiodes in sun sensors.

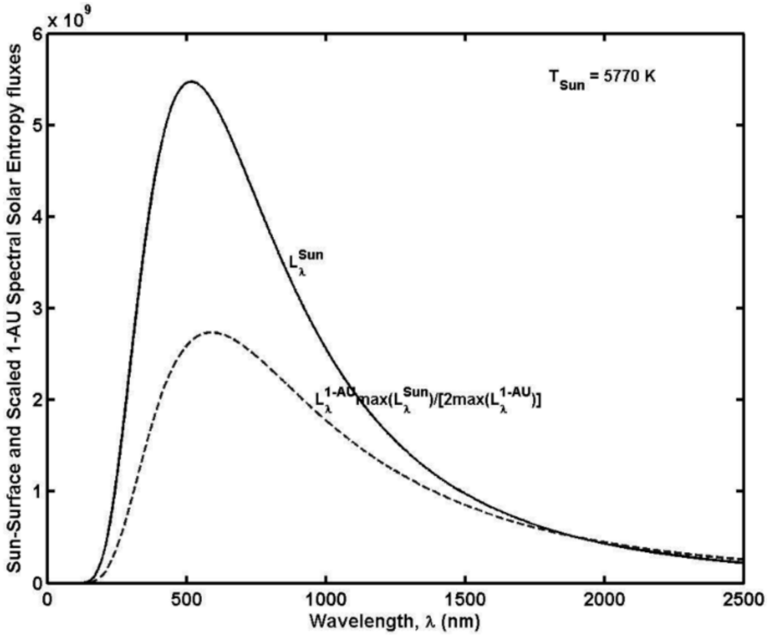

Figure 3: Blackbody radiation of the sun with a temperature of $T = 5770\,\mathrm{K}$. Taken from [12].

The light rays from the sun create two regions of shadow behind the Earth; the umbra and the penumbra. In short; in the umbra region, there is no sunlight. In the penumbra region there is a gradual increase in sunlight the closer to the end of the penumbra region you are. Figure 4 shows a crude illustration of these regions.

2.2.3 Albedo reflection

As sunlight from the sun hits the Earth, some photons are reflected back. The degree of reflectivity is called the albedo, and is based on the color of a surface. The average albedo of the Earth is 0.3, but there are large local variances, as the oceans have an albedo of 0.1, forest can have up to 0.18 and clouds can have up to 0.8. Figure 5 shows the measured albedo of the Earth taken during the entire year 2001.

The albedo of the Moon can also affect sun sensors, but to a much lesser degree than the Earth. The moon's albedo also varies with the different moon phases, and has a maximum recorded value of around 0.14 [9].

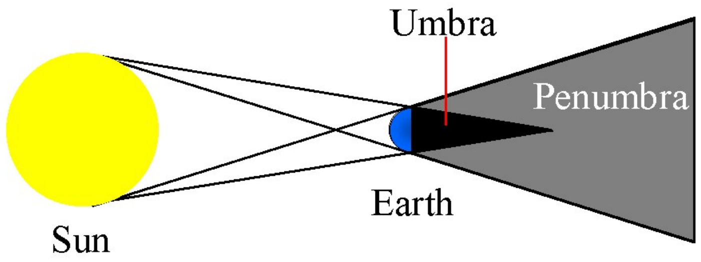

Figure 4: Illustration of the shadow regions cast by the sun behind the Earth

The reflected light from the earth impacts some sun sensors, while others are able to filter, correct for, or ignore the reflected light. Since the albedo varies with both time and location it is not trivial to create sun sensors which are immune from this noise source. In [4], Farian suggests that sporadic events by the Earth and moon's albedo can be ignored by tuning the threshold and timeout values so that the reflected light will be ignored. This is only possible when the sun is out of direct view.

2.3 Sun sensors

To state the obvious, a sun sensor measures the angle of incidence of the incoming light, and outputs a vector between the light source and the sensor's frame of reference. Sun sensors have two primary areas where they are used: Attitude control on sounding rockets, missiles, and satellites, and sun tracking for solar panels.

For attitude determination, the sun sensor is an invaluable sensor, as it uses little power and is reasonably accurate. Most importantly, they do not drift, unless there is some major fault with the sensor. An inertia based attitude determination sensor, like a gyroscope, drifts over time, which make them more and more unreliable for attitude determination as they do not see any external references. Thus, the typical approach is to use a sun sensor or a magnetometer

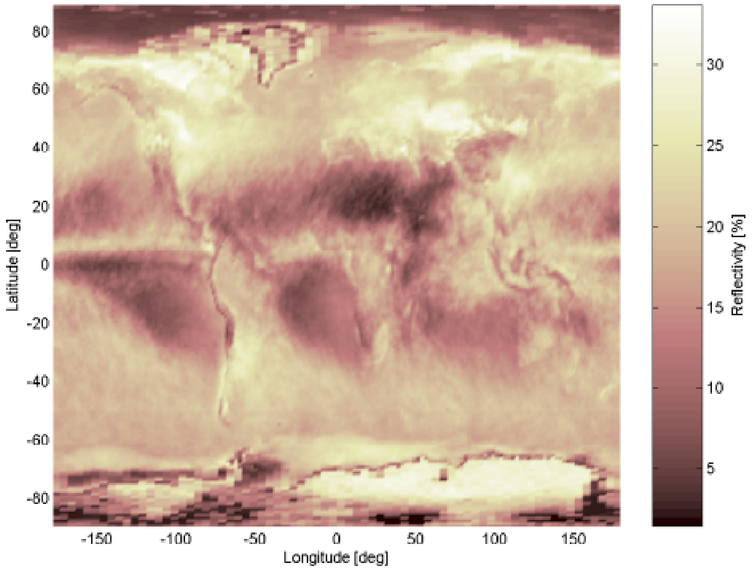

Figure 5: Heat map of the Earths Albedo, taken from [2]

to correct for the drift periodically. As most low cost satellites operate in a low earth orbit [3], they are on the umbra or penumbra (night) side of the Earth almost 50 percent of the orbit. During these parts of the orbit, the sun sensors cannot be used for attitude determination nor control, and therefore most satellites cannot solely rely on sun sensors. In short, sun sensors are used when the sensors can see the sun, inertia sensors are used when the satellite cannot see the sun.

2.3.1 Sun sensors' role in attitude determination systems

Sun sensors are one of the main components in the attitude determination systems on low cost satellites. The sensors range from very crude and simple 1 axis systems reading out the solar panels' output voltage [2], to Mega-pixel digital imaging sensors [13], and everything between. Typical attitude determination systems on low earth orbit satellites have sun sensors facing away from all 6 sides of the structure. Sun sensors are often complementing a magnetometer system, and/or an inertia sensor. As previously mentioned, it is difficult to solely base the attitude determination on sun sensors, as all orbits (other than sun synchronous orbits) will experience that the sun is eclipsed by the earth. While seeing the sun, however, the accuracy provided by the sun sensors and their lack of drift are rivaled only by complex and expensive star trackers.

2.3.2 Imaging sensors

The basis for most sun sensors is found in traditional imaging sensors. Hence, it is useful to use imaging sensor theory as the foundation before discussing on sun sensor specific constraints and concepts.

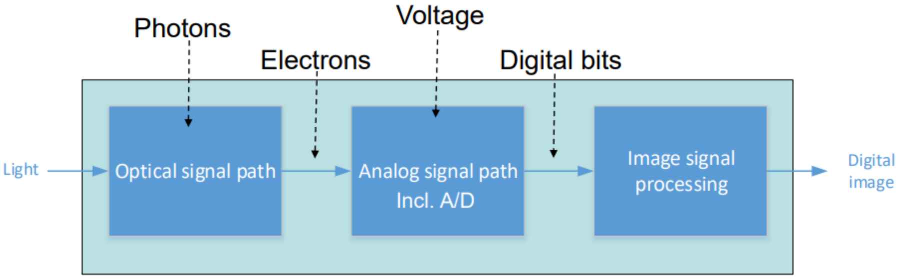

Figure 6: simplified signal chain overview for a CMOS imaging sensor, taken from lectures in in5350

As seen in figure 6, a digital CMOS imaging sensor converts light from a scene into a digital image of said scene. The photons are funneled into the sensor with the help of optics. The optics are used to gather as much photons as possible, increase the field of view, provide an optical zoom, and set the focus point. Optical color filters are often used to let each individual pixel only be exposed to photons with a certain wavelength.

The term *pixel* is used to describe the electronics used to convert the energy from the photons into an electrical charge by employing the photo-electric effect. A simple pixel have four parts: A light sensitive device generating charge based on the incoming photons, a way to integrate said charge over time, mechanisms for resetting the charge to a known level, and an output stage, buffering and/or amplifying said charge level to a signal to be sampled.

A pixel accumulates charge in a capacitance over a set exposure time. This capacitance is often realized by the parasitic capacitance from the gate on the source-follower. The resulting voltage drop is then amplified and buffered onto a bus of multiple pixels' output, where an analog-to-digital converter (ADC) reads the analog signal. This is referred to as a *pixel row.* The ADC's output is then read and processed by some processor or digital logic. One pixel row is read at a time, with a dedicated ADC per column, making the image sensor‘s frame. The time used to read all rows gives the number of frames the sensor can output per second and is referred to as the *frame rate.*

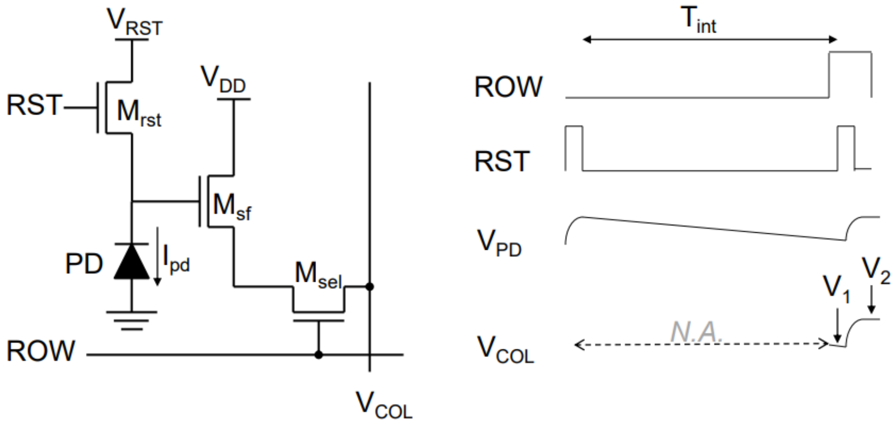

Figure 7: A typical three transistor pixel design, with the corresponding timing, taken from lectures in in5350

2.3.2.1 Photodiode

The building stone of all pixels, and thus sun sensors, are the photodiodes. They are the interface between the photons and the resulting electrical charge. The dimension and material of the photodiode are the primary parameters which govern the response of a photodiode. The area of the photodiode dictates the *quantity* of photons that have a chance to interact with the semiconductor, while the depth of the photodiode dictates the *probability* of a photon hitting an electron, resulting in the photoelectric effect.

Photons with enough energy create an electron-hole pair when being absorbed by a semi conductor. When these electron-hole pairs are generated in a reversed biased PN-junction, a charge is generated as the electron-hole pair is not able to interact. The energy required for the photon to create an electron-hole pair is called the *bandgap energy* and is different for each of the semiconductors.

The chance for interaction between a photon and the PN-junction is called the *quantum efficiency.* The depth of the semiconductor plays a large part in the quantum efficiency, as the photon will have more chances to interact with a medium the more medium it needs to travel through. Thus, the quantum efficiency can either be expressed as the average for the light spectra the pixel is able to detect, or for specific narrower wavelengths.

As stated in [4], the depth of the photodiodes is not disclosed by the silicon fabrication house for the sun sensor, so in this work the typical spectral response of silicon, as seen in figure 8, is used as a stand-in. As illustrated in this figure, the silicon photodiode is sensitive in the most prominent wavelengths of sunlight, making silicon based semiconductors the primary choice for everyday use imaging sensors.

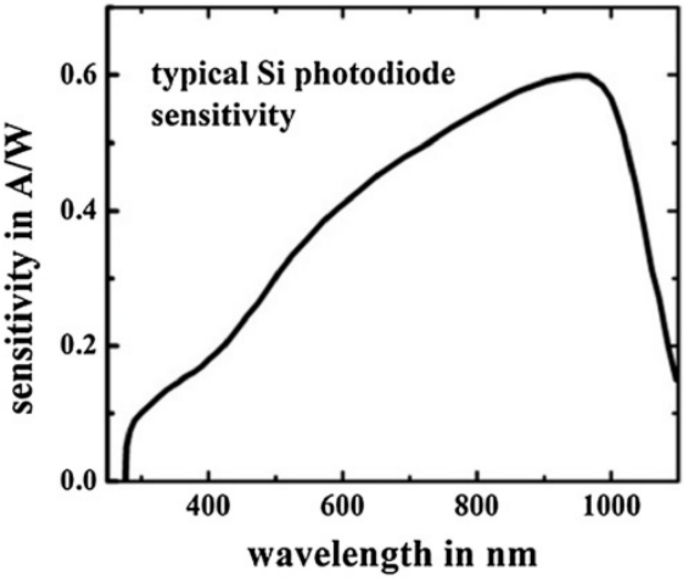

Figure 8: Typical spectral response of a silicon photo diode in photo-current mode. Taken from [8].

Photodiodes are subject to a temperature dependent noise current called *dark current*. This noise increases exponentially with temperature.

2.3.3 Analog sun sensors

In order to provide context to the event based sun sensor, the working principle of more traditional types of sun sensors should first be briefly explained.

2.3.3.1 Cosine sensors

The simplest form of a sun sensor is a cosine sensor, consisting of a photodiode measuring the resulting charge the photoelectric effect provides. These sensors are often referred to as coarse sun sensors The sensors assume a constant illumination from the sun in the form of the solar constant, and any deviation from this is interpreted as a rotational offset from the sun due to the cosine law. The problems with these simple sensors should be apparent; The direction of the angle of incidence is not given by the sensors, they are highly susceptible to aging effects in the form of reduced quantum efficiency, and they are heavily affected by the reflection of the atmosphere of the earth in the form of the albedo effect.

The primary benefit of these sensors is that the solar panels of a satellite can be repurposed to act as a cosine sensor[2, 11], and by using cosine sensors at all sides, the direction of incidence can be derived. As these sensors do not rely on any pixel shading between different sensor elements or pin-hole, but only the cosine law, these sensors are not accurate.

Both cosine sensors and illumination ratio sensors have their resolution directly controlled by the resolution of the analog to digital converts in conjunction with the noise floor found on these signals. Both sensors are also susceptible to albedo reflection

2.3.3.2 Illumination ratio sensors

The most typical type of analog sun sensors consists of multiple photodiodes pointed in the same direction, with some sort of mechanism creating shade on some of the photodiodes based on the angle between the sensor and the light source. These sensors are subject to the cosine law, but since all the photodiodes have the same angle of incidence, the cosine law does not affect the output signal, which is the ratio between the photodiodes.

These sensors (often referred to as fine sun sensors) are able to achieve a much better accuracy than simple cosine sensors, but like cosine sensors they require a calibration process to get desired performance. As the output is a ratio between elements, the elements themselves must be either matched, or characterized and compensated for, to create the correct ratio of all angles of incidence. As the response of a photodiode is affected by the temperature, such sensors' photodiodes should also be characterized over the relevant temperature range. An example of such a sensor can be seen in figure 9.

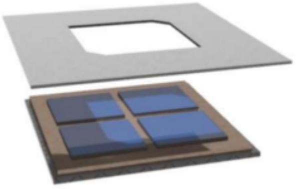

Figure 9: Illustration of analog sensor concept with different degree of illumination on four photodiodes, taken from [1].

Both the coarse and fine analog sun sensors aims to have large photodiodes, to get the best sensitivity, and thus better accuracy and/or resolution if paired with a high resolution ADC. Small fine sun sensors can have photodiodes with an active area of 2.25 mm^2 [1], but can also be much larger.

2.3.4 Digital sun sensors

A digital sun sensor works much like a typical imaging sensor found in digital cameras. The pixel design and layout is generally identical, and digital sun sensors have greatly benefited by piggybacking on the development of terrestrial imaging sensors. The pixels are read out in rows to form the entire frame, before the data is processed. Digital sun sensors do not require color filters, and can operate with monochrome scenes. Digital sensors are typically slower than their analog counterparts, as they have more data to read out and more to process to produce a vector. Digital sun sensors try to locate the center of the group of most illuminated pixels on the frame, and based on the pixels' location they can output a vector to the illumination source. Exposure time and gain can be highly optimized when using optics with a small pinhole, such that only a small group of pixels is actually exposed to light. Even when using such optics, the entire frame is still read out, making the typical performance of such sensors slow, and/or power hungry compared to analog sensors. Due to the vast difference in quantity of pixels (hundreds of thousands versus four), digital sensors have a much higher calibration potential, where the response of each pixel to a reference light can be evaluated and compensated for. Dark current generated from temperature should also affect the output less. Digital sensors are therefore generally able to be more accurate and offer a better resolution with more immunity to noise than analog sun sensors, but are more complex.

Digital sensors aim to increase their resolution by having small pixels close to each other, typically lower than 150 $\mu\mathrm{m}^2$ per pixel to have high pixel density. Resolution can be increased by increasing the amount of pixels and having a larger distance between the pixels and the pin-hole, but by increasing the amount of pixels power consumption goes up and frame-rate is typically lower.

2.4 Event-based sun sensors

This subsection tries to provide a deeper dive into the event based sun sensor. First the basic working principle is given, then different aspects of the sensor is described before a detailed explanation of the modes and the resulting output data sensor is showcased.

2.4.1 Basic working principle

The event-based sun sensor is a sun sensor inspired by the working principle of the human eye, with several neurons firing a signal independently of each other, which creates asynchronous data. For the sun sensor, each pixel is analogous to a neuron, where an interrupt signal is generated when the pixels see light. In this work, *events* are pixels that *triggers* when they have been exposed to enough photons. A closeup of the actual sensor Application Specific Integrated Circuit (ASIC) can be seen in figure 10.

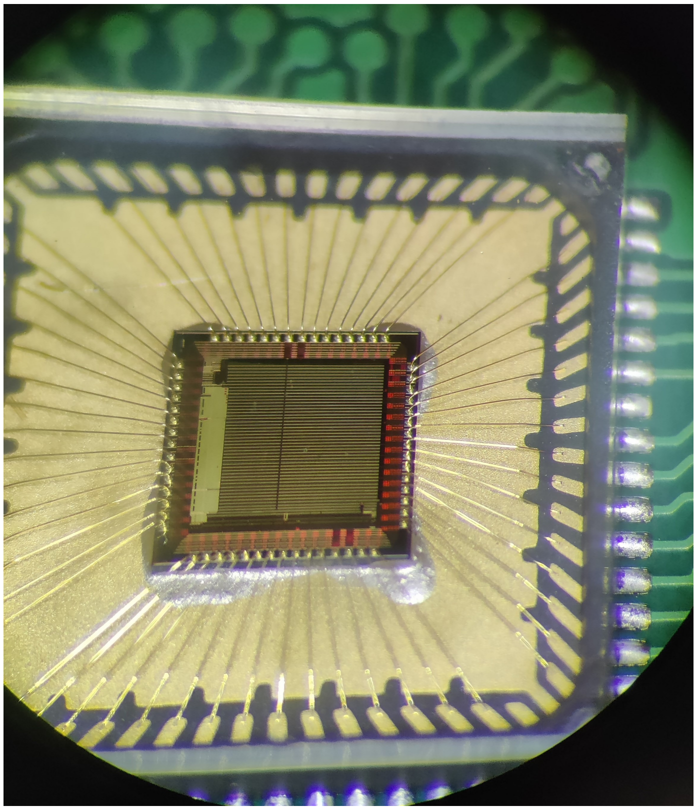

Figure 10: Close-up of sun sensor ASIC with glass lid without slit optics.

The sensor as it exists currently outputs pixel locations on two independent buses; one for each axis. To produce the sun vectors, the sensor must be controlled by a readout system acknowledging the incoming data, but also setting digital control pins and analog bias voltages. The sensor foregoes both the full pixel frames found in digital sun sensors and the photodiode quadruplet found in analog sun sensors for a 2 pixel line design, as seen in figure 11. The two pixel lines operate as two independent sensors with their own control and data interfaces. Said design requires a corresponding pin-hole like optics, and the neuron inspired independent pixels call for new non-typical readout and data processing to fully utilize the novel sensor concept.

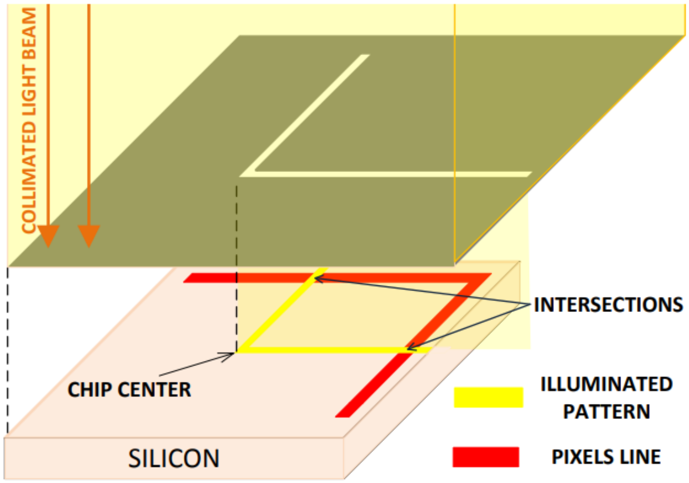

Figure 11: Illustration of sensor concept with slit optics and pixel lines.

2.4.2 Process and packaging

The sensor silicon die made with AMS 0.35 µm CMOS image sensor process is mounted into a QFN-64 package's ground pad via adhesive on the die's corners. The die is bonded to the package via what appears to be typical gold bonding wires. The process uses an extra anti reflective coating to get more responsive photodiodes [4].

2.4.3 Optics

From the fabrication house the sensor has a clear glass lid secured with brittle adhesive on the top of the QFN package. A new glass lid with a metalized side was designed for the sensor with a slit to provide a directional light. As the optics are flat, they will provide no focusing, magnifying or other refraction of the light. As the same medium is on both sides of the optics, the angle of incidence is not changed, but the light is very slightly shifted due to Snell's law, as seen in figure 12

Figure 13 shows the optics in a top and side view. The slit's L-shape is inverted from the L-shape made by the pixel lines to ensure that only a handful

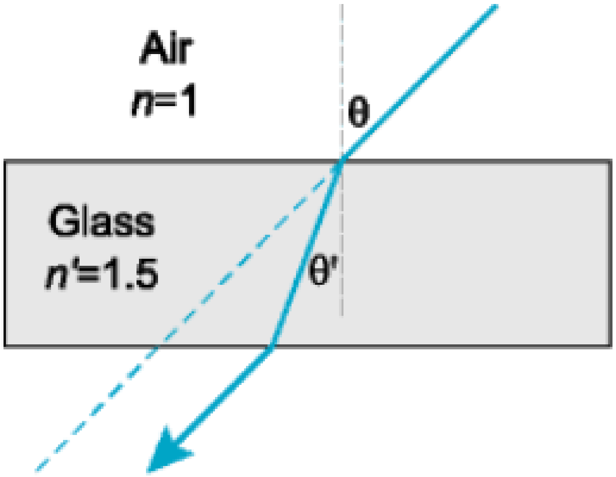

Figure 12: Light refraction example from air to glass back to air, taken from [10].

of pixels are illuminated at the same time. The dimensions for the optics are L = pixel length = 2256 µm, h = slit thickness = 100 nm, w = slit width = 50 µm, d = Focal distance = 356 µm.

2.4.4 Pixel design

The pixel design for the sun sensor is different than on traditional sun sensors and other imaging sensors. Where a normal pixel would output an analog signal to the pixel array bus to be converted into a discrete value, this sun sensor pixel implements more logic into the pixel.

As can be seen in figure 14, the working principle of the pixel has the normal photodiode and reset transistor, but replaces the typical follower with a differential amplifier used as a comparator. This comparator sends out a digital high signal when the pixel charge crosses the threshold set by the external threshold pin. As the charge will steadily keep flowing, the comparator will keep outputting the same signal until the pixel charge is reset via the reset transistor.

The location, as a pixel address, is then determined by a bus arbiter, which in turn is transferred as the output address on the bus. When the external data-bus has acknowledged the data from the pixel, the pixel is then reset. How the arbiter determines which address to output if there are two or more requests waiting while handling an earlier pixel's output request, is not clear from [4],

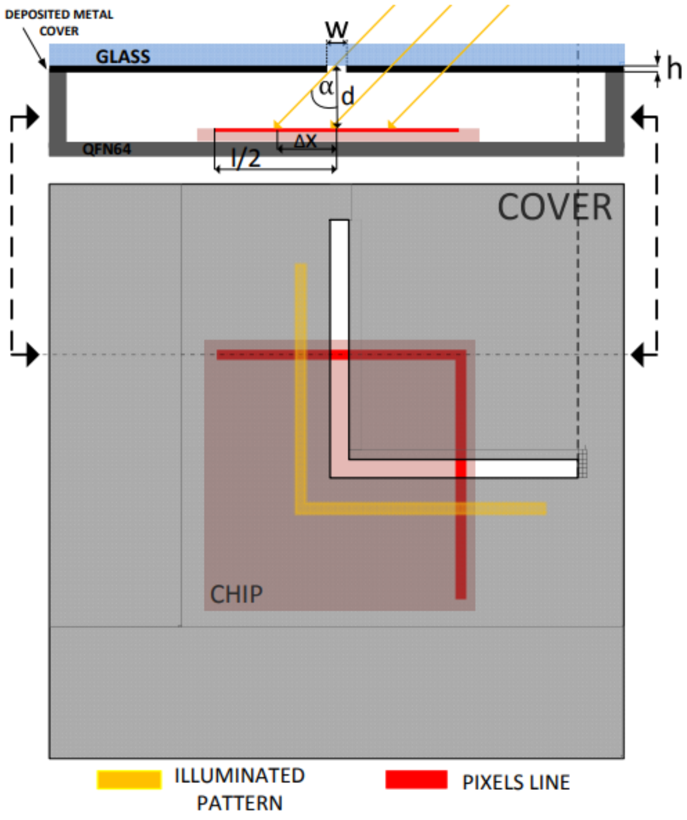

Figure 13: Top and side view illustration of the optics mounted on the sensor, taken from [4]

as there does not seem to be any queuing system. Current best guess is that it is determined based on pixel address, giving a priority to either higher or lower addressed pixel regardless of actual pixel trigger order.

2.4.5 Pixel array

As with the pixel design itself, the pixel array does not conform to neither typical sun sensor nor imaging sensor design. One of the most noticeable differences is that the pixels on the sun sensor are placed in two orthogonal lines instead of an N x M type array. This creates a 2x N amount of pixels instead of N squared or N x M amount of pixels found in other digital sun sensors.

As the slit in the optics generate two lines of light in an L-shape, one pixel

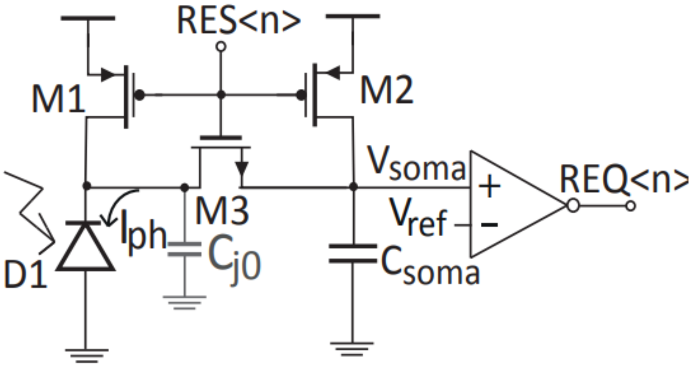

Figure 14: Pixel design taken from [4].

on each line must be read to determine the vector between the sensor and the sun, while traditional sensors would in theory at a minimum only require one. In addition, both pixel lines work completely independently of each other, and have their own set of analog and digital control signals. By using two lines instead of a frame, there are fewer non data generating pixels for each other. Since only the pixels which have been exposed to enough photons to trigger a detection event are read out, the sun sensor is able to operate at a much higher "frame" rate than other sun sensors.

The current implementation of the sun sensor has 192 pixels in each line, with a photo diode center to center of 11.75 µm, giving pixel density of around 88 pixels per mm, or a pixel size of 846 μm^2. Increasing the pixel density should have a negligible impact on temporal resolution, as pixels operate independently instead of sequentially in rows.

2.4.6 Data bus and format

The Asynchronous Event Register bus (AER) was first proposed in [5]. It is a simple bus with handshakes and 4 phases : Idle, data valid(bus_req), data read(bus_ack) and release). The protocol can be modified to support multiple senders and receivers. The AER bus is used to transmit address data from each axis on the sun sensor ASIC to the readout system. The timing and the different phases of an AER transaction can be seen in figure 16 and table 1.

First the sender outputs the data on the bus, then pulls the request signal low to indicate that the data on the bus is now valid to be read. The reader then pulls the acknowledge signal low to indicate that the data has been read successfully. The reader should wait to release the acknowledge signal until the sender has released the request signal first, but this is not a hard requirement.

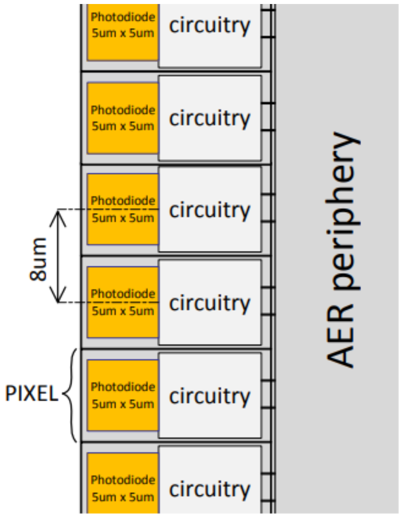

Figure 15: Illustration showing the pixel layout taken from [4]

	min	max	avg
t_1	0 s	∞	
t_2	0 s	∞	$\leq$ 700 ns
t_3	0 s	∞	
t_4	0 s	100 ns	
t_5	0 s	100 ns	
t_6	0 s	∞	

Table 1: Timing of an AER bus transaction. Values are from [5].

Refusing to pull the acknowledge signal low is a simple way to post-pone or freeze the transaction from the sender.

AER does not specify the bus width, but the current implementation of the sun sensor uses an 8 bit width to communicate which of the 192 pixel addresses had an event.

2.4.7 Modes and operation

The sun sensor itself is a relatively ”dumb” sensor which requires some control and management to fully operate. This is done through analog inputs and digital inputs and outputs. The sensor has the following control pins not related to data bus seen in table 2

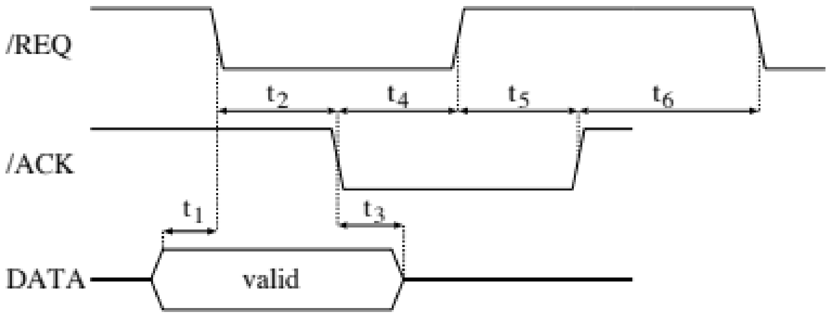

Figure 16: Waveform of a AER bus transaction taken from [5].

The sensor has different modes it can operate in. Table 3 lists the modes and the corresponding digital input needed to activate each mode. When the global reset signal is high, all sensor operation is halted by keeping the pixel reset active. By disabling the timeout and counter functions, the sensor enters what is referred to as *normal mode* in [4]. The term *free-running* is also used for this mode. In this mode there is no coordination between the pixels in a line; when a pixel's charge reaches the line threshold, it triggers, holding the AER data bus until it is read out, then only is the triggered pixel reset. In this mode, given enough time, all pixels should trigger at some point, as a result of dark currents. Due to this, sporadic (false positive) triggers not related to the sun vector will eventually transpire, and thus a readout system should actively use the global reset signal periodically.

Timeout mode is this first viable mode of operation. The mode aims to remove sporadic triggers by applying a reset when an internal capacitor discharges down to a threshold level. The capacitance is recharged when the global reset is active. When tuned, only the illuminated pixels should have had the chance to trigger before unrelated pixels. If the timeout is long enough, the illuminated pixels can trigger multiple times. When in timeout mode, the sensor's event threshold level sets the minimum *charge level*, but the Timeout bias pin (V_timeout_threshold) sets the *maximum time for a pixel to reach* this level of charge. This means that both can be used to set a floor on what illumination level the sensor should react to, and what is considered unrelated triggers.

The last mode is the *Time-for-n-spike* (TFnS). By setting the CNT_DIS, the counter block is activated. As opposed to in free-running mode and timeout mode, a pixel is only allowed to trigger once until the pixel line is reset. When the internal counter has reached the number of triggers set by the select pins (see table 2), the pixel line is reset. When reset, the pixel address 0x00 is outputted on the AER data bus. The resulting set of samples delimited by the 0x00 pixel

Pin	Function	Default value
PDx	Pull-down bias for data bus 1 and 2	0.9 V
PUx	Pull-up bias for data bus 1 and 2	2.6 V
Global rst_x	Global reset (one pixel line) for line 1 and 2	Float
Timeout_Disable	Digital control for the pixel timeout function	High
TFS_Disable	Digital control for the winner takes all mode	Low
Sx	Selection for the amount of winners in winner takes all mode 0x0 =1 0x1 = 2 0x2 = 4 0x3 = 8 0x4 = 16	0x0
V_threshold_x	Sets the threshold level for all comparators on a pixel line. Lower voltage means larger distance between supply and threshold	1.30 V
Follower_bias	Analog bias for source follower	1 V
V_timeout_discharge_x	Analog bias, sets discharge rate for timeout capacitor	0.22 V
V_timeout_threshold_x	Threshold for timeout to trigger	1.15 V

Table 2: Table of non data bus pins on the sun sensor, and their function.

Time_DIS	CNT_DIS	GLOB_RES	Mode
X	X	1	Pixels in reset
1	1	0	Free-running mode
0	1	0	Timeout-mode
1	0	0	TFnS
0	0	0	TFnS + Timeout

Table 3: Digital control over sensor modes.

is henceforth called a cluster.

When the select pins only open for 1 trigger, the sensor operates on a winner takes all principle; the most illuminated pixel will be the first to trigger. The most illuminated pixel should be the one that is less shaded by the optics, and hence the vector can be derived based on said pixel's location. As only one pixel is allowed to trigger before the counter reaches its maximum, all pixels on the line is then reset. I.e., only the winning pixels are allowed access to the bus.

By increasing the counter's maximum, the sensor now operates on a *multiple winners*-winner takes all principle. As seen in figure 17, more than one pixel will see some light and therefore the most illuminated should trigger first, followed by neighbors on both sides. By looking at the median of the pixel address, the

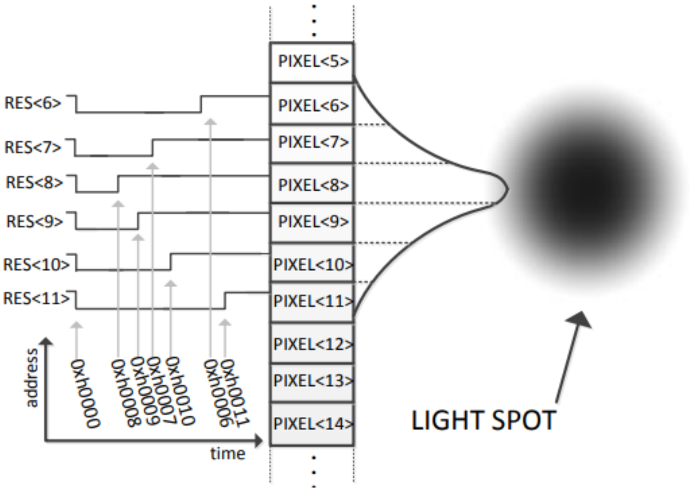

Figure 17: TFnS operation illustrated taken from [4].

center-point of illumination can be found. This mode can help to correct for uneven pixel response, at the cost of latency. TFnS can be combined with the timeout function. Using multiple winners the sensor can generate larger clusters for data.

2.4.8 Performance

In [4], several tests have been performed on the sun sensor. During these tests the sensor has been able to produce 11k events per second, and has a field of view of 120 degrees. The accuracy vs angle of incidence is only given as two ranges, one where the angle of incidence is smaller than 60 degrees, and another where it is larger than 60 degrees.

The sun sensor has its performance listed in events per second. This is not the most transparent way to represent the temporal resolution, as the readout system needs an event per axis to determine the sun vector, and both axes could have a different rate of events per second as well, due to the cosine law. Then, when factoring in Winner takes all mode, where multiple events are applied without resetting the pixel line between each event, the "events per second" becomes a muddy and imprecise metric for determining the temporal resolution of the sensor.

3 Models

The models presented in this text have been created on the basis of [4], which describes the ideal angular output. Models in this work is either from the original source, or expanded upon or derived from observations of the sensor. The models are used to set the expectations for the behavior of the sensor, and to further refine the data via processing. Based on the results, the accuracy of the models will be discussed.

To be able to make any meaningful calibration and characterization, a model of the sensor should be made. The most important part of this is the angle of the light source vs the pixel address seen in equation (3) and the maximum field of view (4).

3.1 Output vector models

$$Output\theta = tan^-1(\frac{(Pixel_{address} - Pixel_{center}) * Pixel_{pitch}}{Height_{slit}}) \tag{3}$$

$$FOV = 2 * arctan(\frac{Pixelarray_{length}/2}{Height}) \tag{4}$$

Another model that can be explored is the sensor's events per seconds vs sensor illumination, based on (5). This model can then be further refined by taking into account the angle of the light source, as it will affect the quantity of events negatively with increased angle, as per cosine law.

$$T = \frac{(V_{DD} - V_{ref}) * C_{tot}}{I_{ph}} \tag{5}$$

$$F_{ocs} \approx \frac{I_{ph}}{(V_{DD} - V_{ref}) * C_{tot}} = \frac{I_{ph}}{C_{ph} * \Delta V} = \frac{1}{T} \tag{6}$$

Changing the current I_{ph} to be dependent on the angle of incidence, we get the following equation for frequency (7):

$$F_{ocs} \approx \frac{Imax * cos(\alpha_{incident})}{C_{ph} * \Delta V} \tag{7}$$

3.2 Latency models

As temporal data in the form of sample and cluster latency is interesting data to derive from this particular sensor, two models are proposed; One for a macroscopic view over the entire field of view, and one microscopic model focusing on only a few neighboring pixels.

The macroscopic model is based on the expectation of 11kilo samples per second (kSps) when the light is centered, then decreased by the cosine of the angle of incidence in both axes. Figure 18 shows this in a 3D plot where the Z-axis is the inverse of samples per second.

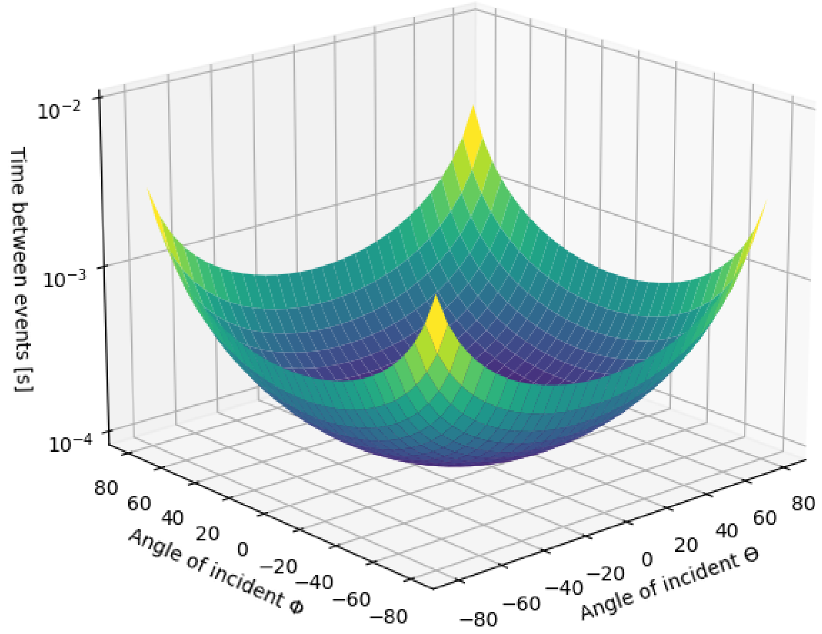

Figure 18: Plot of expected delay between events. Here the Z-axis is on a log scale.

The microscopic model tries to capture the small wave-like changes in latency. The idea is that when the incoming light fully envelops a pixel, it charges in its ideal time frame. When the angle of incidence is slightly changed, the pixel would no longer be fully enveloped, but only partial. Note that the change of incidence is less than the resolution, meaning that the sensor will output the same pixel address as data. When the pixel is only partially hit by the incoming light, the time the pixel needs to charge its internal capacitance increases. This keeps increasing until the neighboring pixel is now more illuminated than the original pixel. Due to the abrupt change in which pixel is most illuminated, the resulting latency pattern looks like a series of triangular waves which have their peak slightly raised the further from the center pixel the corresponding pixel is located. The ideal latency for one pixel is around 88 µs. From Figure 22, we can see that this increases by around 60 % to 140 µs. Simplifying the change as a linear rise and fall the latency for one pixel then becomes:

$$Pixel_{locationlatency} \approx Min_{latency} + Min_{latency} * Cos(\alpha) \tag{8}$$

$$Pixel_{latency} \approx Pixel_{locationlatency} + Tan(\alpha) * Max_{latency} \tag{9}$$

3.3 Error

Due to the combination of even pixel pitch, flat optics and trigonometry, the sensor has an error noise, which gives poor performance in the area of view most sensors have the best performance.

1° change in angle of incidence has a much larger distance impact near the center pixel, than the pixels near the end. With a constant pixel pitch, this means that a larger change in angle is needed before the neighboring pixel sees the majority of the light near the center than at the pixel line end. The relationship between angle of incidence and distance from center can be seen in expression (10).

$$\Delta Distance = Tan(\alpha) * Optics_{Height} \tag{10}$$

Due to how close the optics are to the pixels, compared to the pitch, this means that the sensor ends up with a worst case resolution at 1.88° near the center, but 0.22° at end of the pixel line. Figure 19 and 20 shows an illustration of this.

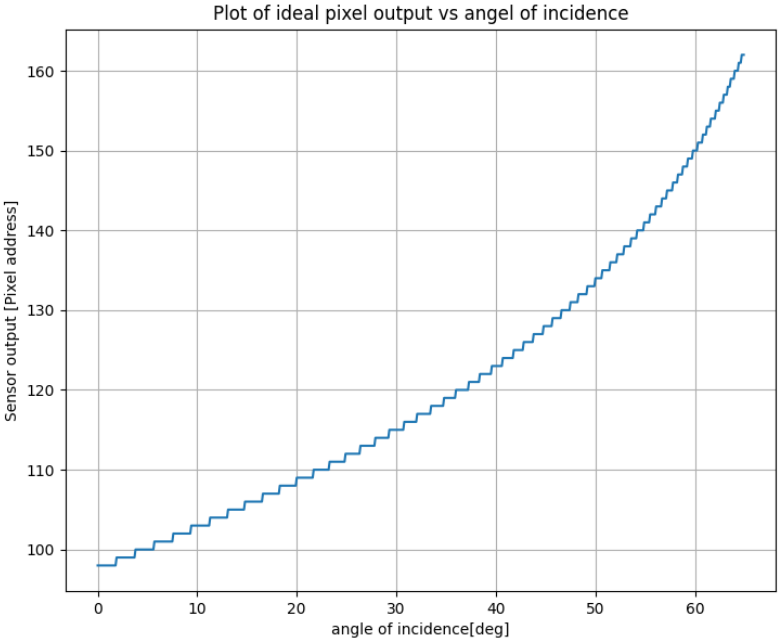

Figure 19: Plot showing quantization noise and how the resolution increases with angle of incidence

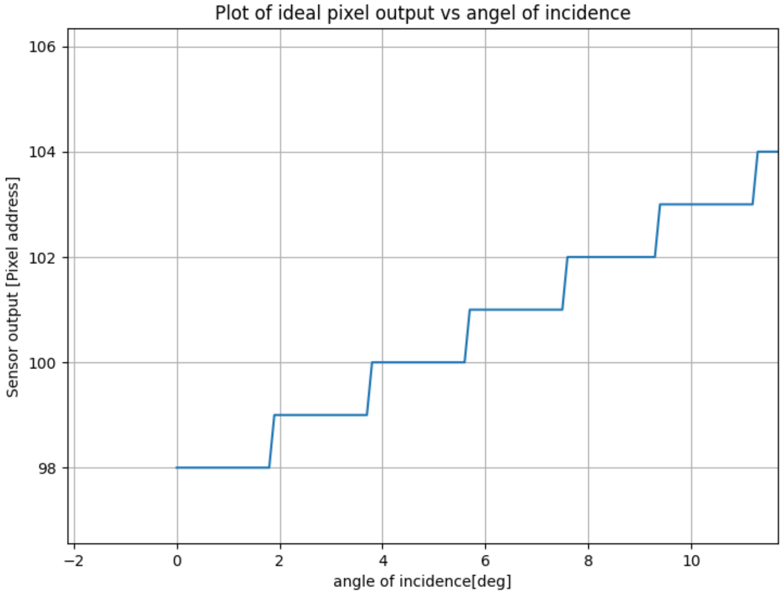

Figure 20: Zoomed in view of figure 19 showing the quantisation effect

This also results in more pixels being hit by the incoming light when the angle increases, which is relevant for the *Multiple winner takes all* mode.

Another major source of errors on the sun sensor is found in the actual assembly of the sensor. The output address of the pixel the sensor gives out at normal angle of incidence is dependent on the placement of the optics in relation to the silicon die. The placement of the silicon die on the current iteration of the ASIC is not controlled. It is simply placed near the center of the package and secured via adhesive to the surface. This gives ample opportunity to have some shift and misalignment in the die placement. The placement of the optics likewise affects the *normal incident* address, or rather the placement of the slit. These alignment errors and variances manifest as offsets in the output address of the pixel, which can be easily corrected. This error also *eats* the FOV from one direction without necessarily giving the same amount of FOV back to the other direction.

[4] claims that misalignment between the slit and the pixel rows contributes up to 2.83 degrees error, which seems to only consider the production tolerances and does not include the manual assembly. The main take-away is that the sensor seems to be susceptible to offset errors.

Misalignment in the form of a rotated slit in relation to the pixel line on the silicon die could also affect the response. This would manifest as a non-linear error instead of a linear offset. Intuition says that the rotational offset should be great before impacting the sensor drastically. This can be seen in expression 11 below.

$$\Delta Pixel_{rotation\theta} = \frac{Pixel_{length}/2 * tan(\theta)}{pitch_{pixel}} \tag{11}$$

A 1 degree misalignment could thus result in a two pixel offset.

4 System Design

A control and readout system is designed for dual use; both in lab and in situ. These uses have their own set of requirements, but the end result does not suffer because of this. The readout system should be able to affect all aspects, pins and modes for the sensor. The readout system should also limit affecting the data or in other ways induce some bias to the readings. Lastly, as the electronics of the readout system had to be designed early, as manufacturing take time, the electronics design was executed with the philosophy that the whole design could be wrong and full of errors, but that it should be fixable with bypasses, or configurations.

A major part of this work is the design of one system capable of reading and controlling the sensor ASIC for both lab tests and in situ experiments. The lab experiments revolve around two types of tests; characterization of sensor performance with standard use for calibration purposes, and data gathering of new applications of the sensor. For in situ experiments, a reference sensor is needed, and the system must be able to both produce large quantity of raw unprocessed data as well as processed and filtered low quantities of data in a space environment.

4.1 System Components

4.1.1 Sensor board

The sensor board is the circuit board containing the sensor, the ASIC, the temperature sensor, and digital to analog converters for the analog bias voltages. In case there is a production fault with one of the ASICs, changing the sensor board is easier than changing the entire set of electronics. The original idea was that only one main board could be used to calibrate multiple sensors boards. After the sensor board has had its components soldered, the clear glass lid of the original ASIC packaging is removed and replaced with the glass lid with a metalized side with the corresponding slit. The optics are aligned with a 3D printed jig, which is in the shape of a cross, so that the corners of the glass and the packaging is not covered. Then the glass lid is secured with epoxy on the corners. Epoxy is specifically used due to its flexible nature to allow some temperature expansion.

4.1.2 Main board

The main board contains the support electronics for the readout system.

4.1.3 Reference sensor

The readout system has a reference sun sensor. This is a commercial analog fine sun sensor, typically used on small CubeSats. It is powered with 5V, and has an I2C interface. To operate it, a sample command must first be sent, after which the master must wait at least 30 ms before reading out the sample. The output is given as 4 photodiode voltages, and the master must then convert the ratio into a sun vector. The reference sensor is supplied with a lookup table for calibration values for 81 points on both azimuth and elevation angles.

The reference sensor is used to verify the alignment between the light source and the readout system in an efficient manner. The reference sensor also acts as a performance guidance. Lastly, the reference sensor is used in the in situ experiment to give an "apples to apples" comparison on how the sun sensor performs, as previously mentioned.

The sensor data sheet lists that it has an accuracy(when calibrated) of $< 2°$ when angle is $> 45°$, and $< 0.5°$ for the rest. It has a theoretical maximum sample rate of 33hz, and a field of view of 120 °.

4.1.4 Enclosure

The readout system has an aluminum frame that acts as an enclosure for the electronics and the reference system. This in turn can be mounted on a 3D printed jig, which interfaces to the spin table seen in the test setups in section 9. Said enclosure keeps the sun sensor and the reference sensor pointed in the same direction parallel to each other.

4.1.5 Angular correction via temporal data

As noted multiple times during this work, one untapped feature of the sensor is that vector data is not the only data produced, but also temporal data in form of time delay between samples. This data should not be wasted, but rather repurposed. This subsection proposes a method to use the timing data to make the sensor act as a type cosine sensor. Instead of output charge, the timing data is used to provide an additional angular measurement, which then could be combined with the primary vector to potentially achieve a higher accuracy.

As can be seen in figure 21, the latency, as expected, is lowest when the angle is normal to the sensor, and increases the further away from 0 the angle grows. What is less expectant is the variance in latency. The variance is most present and scattered when the angle is at its smallest. This is fortunate, as according to the stated performance, the accuracy falls the further the angle increases from 0.

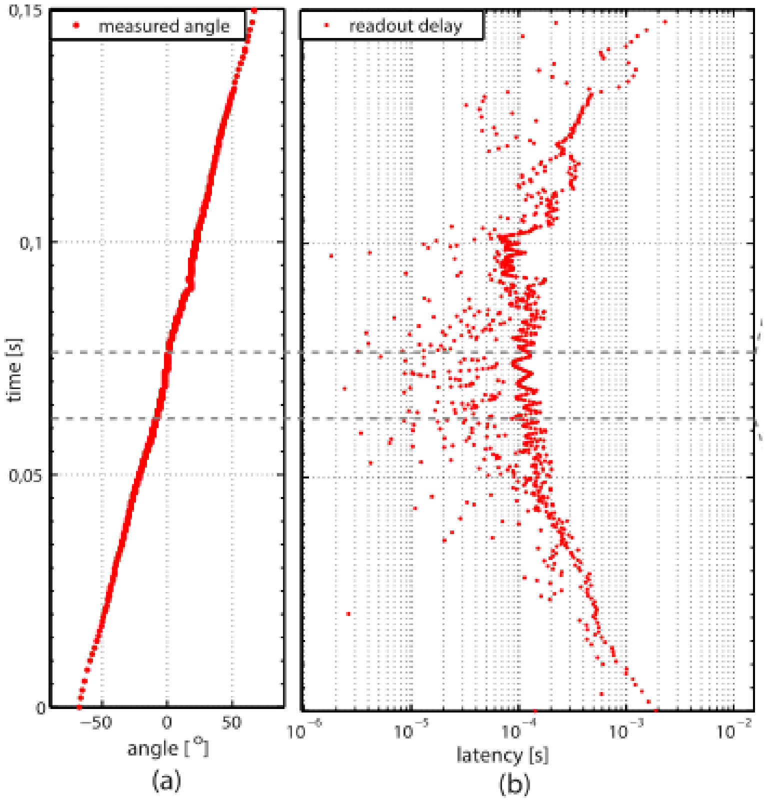

Figure 21: Sensor output angle and latency, taken from [4]

Figure 22 shows on the right side how the latency follows a wave pattern. By gathering the latency of a cluster of samples instead of only one sample, the expectation is that a more defined latency pattern will emerge. To save time implementing, angle correction is attempted in post processing with scripts parsing the raw data.

4.1.6 Resolution increase with temporal data

As we can see, by receiving temporal data in additional to angular data, in theory, the resolution can be increased.

Imagine a large single pixel of the same design found on the event based sun sensor. When triggered, based on the pixel location, a vector can be found.

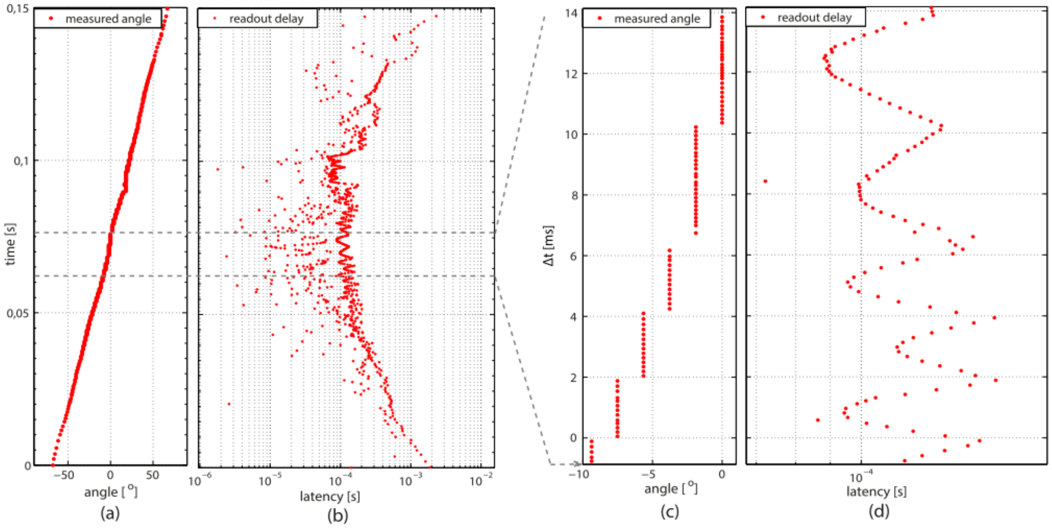

Figure 22: Zoomed in view from figure 21 showing a set of smaller waves in the latency on the right side within one pixel address. Taken from [4]

If the neighboring pixel triggers, an increase of incidence angle based on the pixel is assumed. Any angle delta between the step size based on the pitch is ignored. By saying that there exists a small enough change of angle that will not cause the neighboring pixel to trigger instead of the pixel in interest, the time between two triggers on the same pixel should change in relation to the small angle change proportional to reduced direct illumination.

The stated resolution for the sensor is 0.22° - 1.88°. The resolution is skewed, so that it is at its worst the nearer to normal the angle of incidence is, and is a product of using a pinhole with equally pitched pixels. As seen in figure 22(c), the sensor outputs the same angle multiple times on the Y axis, while the actual angle (x) has changed. The sensor is unable to differentiate angles less than around 1.88°, and it can be observed that when closer to 0°, there are more samples showing the same measured angle than at around 7.5°.

In figure 22 (d), we can see how the latency swings, with its lowest latency in the middle of a group of a series of the same angle outputs, and the latency increases until the neighboring pixel ”takes over the output”. This method seems like it can only be effective up to around 15° deg angle of incidence as each of the latency dips become narrower the further away from 0° the illumination moves.

Thus, the finer resolution for the angle could be expressed as the base location + temporal correction. By comparing the delay for neighboring pixels as well, even greater resolution could be possible. Using the neighboring pixel's output, the direction to offset from the base angle can be determined.

To facilitate this proposed function for higher resolution, time tagging each event as it comes is paramount. As the lowest latency point varies for each pixel, each pixel's time delay and the angle where the neighboring pixel *takes over the output* must be characterized. Due to the asynchronous design of the pixels, the temporal response should act continuously rather than as a discreet function. High resolution temporal data sampling is relatively simple to implement using FPGAs, so this creates the foundation of the readout design:

The readout system must be able to log the incoming data, and only add a known and deterministic latency to the incoming data. The readout system will operate at a clock frequency that is at least two magnitudes faster than the fastest incoming data.

4.1.7 Albedo detection

To detect which body the incoming photons are from, traditional sun sensors try to measure the incoming irradiance, and compare it to the solar constant. If it is more than the solar constant, the on board processing assumes that it sees both the sun and the earth, while if it is much less than the solar constant, it assumes that it sees the reflection from the earth. Typically, sensors would then output an error code together with the data to give a indication that perhaps the data should be discarded, but leaves the decision up to the Attitude Determination and Control System (ACDS). With this information, the ADCS can reduce the confidence applied to the incoming measurements from the sun sensor.

For the event based sun sensor, two techniques to determine interfaces from the albedo of the earth is proposed in this work. The first is similar to the one implemented on traditional sensors; measuring the incoming illumination. The illumination is approximated by measuring the time between two samples. The shorter the time, the higher the illumination. Due to cosine law, the angle of the light needs to be compensated for; the time delta between samples on the center pixels will result in a lower approximated lux than on the pixels closer to the edge. Individual pixel characterization should also be weighted in this calculation.

The other technique is to check for consistent false triggers. Assuming that the slit is sufficiently thin enough, so that the incoming light from the primary light source does not directly hit more pixels than the maximum counter select can support in TFnS mode, the remaining TFnS count triggers should happen on pixels not hit by the primary light. All remaining pixels now race to trigger first, but the pixels illuminated by a weak secondary source should trigger before the rest. If the last set of triggers form a group and is not spread randomly, the sensors have to be able to capture the secondary light source.

Due to time constraints, Albedo detection is just proposed, not implemented.

5 Electrical design

The electrical design for the readout system is not complex, and have been kept as simple as possible. It consists primarily of a flashed based FPGA and the corresponding power circuits. The sensor's data and control pins are directly connected to the FPGA without any buffers between, while the analog bias pins are driven by two digital to analog converters. The readout system also has a small non-volatile data storage device.

To communicate and control the readout system, a 3.3V fast I2C is implemented. As the readout system will also be used on a student satellite, the I2C interface has a bus isolation circuit, which can be used to prevent the readout system from permanently halting the I2C bus in case of a fault. This circuit also increases the current sinking capabilities of the bus, making excess bus capacitance a non-issue when using the I2C fast mode. The readout system is programmed via a dedicated JTAG interface using a flash-pro 4 USB-to JTAG dongle required for the smartfusion 2 FPGA. A debug interface is also present on the same programming connector in the form of a 3.3V TTL UART, as it is always useful during development stages.

Figures 23,24, 25 and 26 shows the different sides of the populated printed circuit boards (PCB), as well as how they stack together to form a low profile electronics system which fits a strict height restriction envelope.

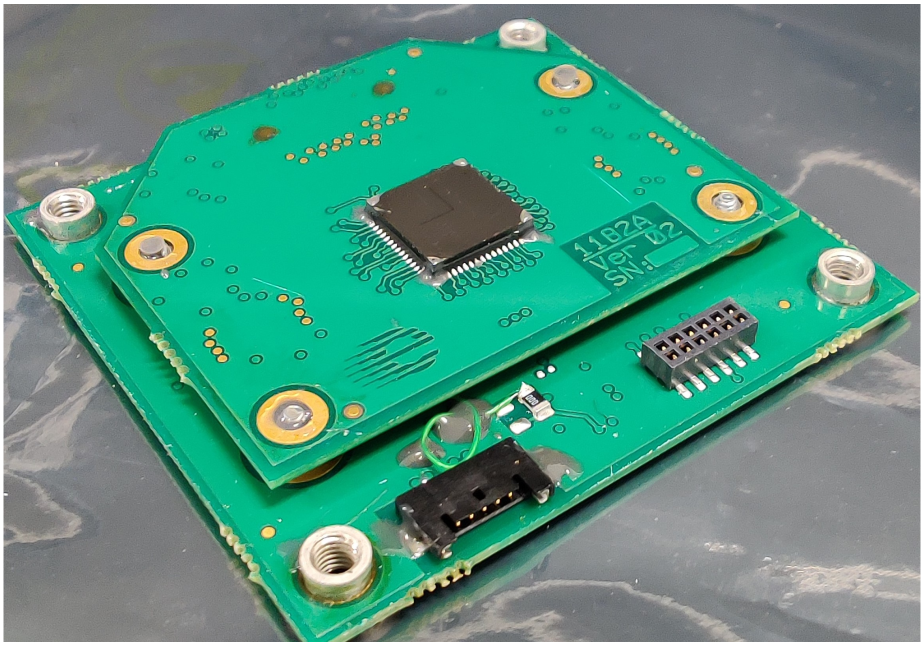

Figure 23: Photo of the two PCBs stacked, Sensor ASIC can be seen with the slit secured with epoxy

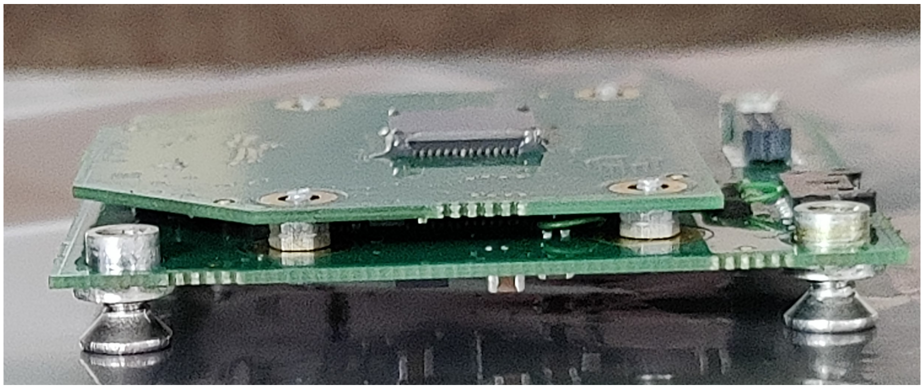

Figure 24: Photo of the two PCBs stacked seen from the side, distance between the PCBs is 2 mm

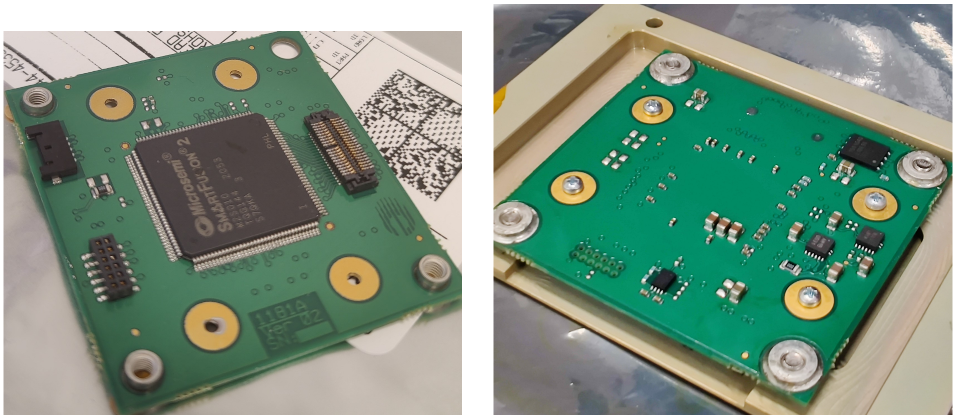

Figure 25: Left: Top side of the main PCB containing the FPGA. Right: Bottom side of the main PCB containing the power and memory

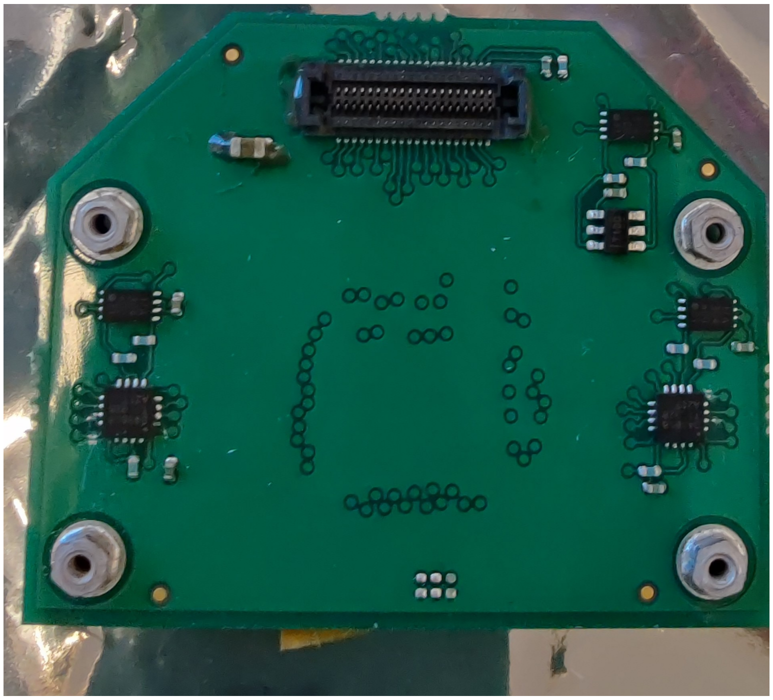

Figure 26: Photo of the bottom side of the sensor PCB, containing the digital to analog converters and the temperature sensor

5.1 Analog Bias

To provide all the analog biases to the sensor ASIC, two 8channel digital to analog converters are placed on the sensor PCB. These digital to analog converters have an I2C interface, in which a separate I2C isolator is used. The Digital to analog converters have an 8 bit resolution, and have their own internal voltage reference. As it is powered by the 3.3 V power supply, the bias can be controlled in 11mV steps from 0 to 3.3V. The package is pin compatible with a 12bit version that can be swapped to if higher resolution is required. The outputs are floating when disabled, but have an internal 10kohm pull down to ground. The current sunken by the sensor on the bias pins is not measured, but the driving capabilities of the converters are adequate, as the output voltage does not collapse.

5.2 Temperature

All lab test have been performed in a basement which holds a temperature of around 20°C. This does not trigger any need for temperature monitoring, but when exposed to the environment found in low earth orbit, the temperature will vary greatly, which in turn could affect how the sensor performs. For that reason, a temperature sensor circuit is included in the design. This sensor is placed on the back of the sensor PCB, where it monitors a copper shape connected to the bottom of the sensor ASIC's QFN package, as the purpose is to get the temperature of the sensor and not the rest of the electronics. Only the sensor will be exposed to sunlight, which can result in a different temperature profile than the rest of the system's components.

The temperature range is a product of the orbit parameters, which are currently not known. Typical temperatures for Cubesats in low earth orbits are however in the range -30°C to 70°C depending on the node. The electronics on the readout system are all rated for -40°C to +85°C, while the sun sensor has currently no temperature rating. Being exposed to temperatures higher than the maximum rating are typically not of a catastrophic nature, but can cause small incremental changes in performance. Multiple temperature cycles, on the other hand, pose a larger strain on the electronics, and the failure mode is typically not a change in performance, but manifests as disconnects on solder and bonding joints.

5.3 Sensor board interface

As the readout system consists of two separate PCBs, there has to be an interface between them. One of the main design constraints for use on the student satellite was limited space when building outwards from the satellite. so the stacking distance between the main board and the sensor PCB had to be small. A board to board connector with a stacking height of only 2 mm from Samtec was used. To provide mechanical relief, threaded board standoffs were soldered on the main board, and small bolts where fastened via the sensor PCB.

The connector between the two boards transfers an I2C bus for the digital-to-analog converters and the temperature sensor, power for the circuits, and data and digital control for the sensor ASIC.

5.4 Power design

The system is fed 5V, but all internal circuits are powered at either 3.3V or 1.2V, This lessens the level requirements for the input voltage. The switching DC/DC converters have some inefficiency when only a small load is drawn.

The readout system does not contain any circuit breaker or fuse mechanism, but both the DC/DC converters have an over current protection, which should prevent critical damage for most accidents during testing. The system does not have reverse polarity protection.

5.4.1 Lowering the power consumption

While commercial sensor producers often strive to make their sensors consume as little power as possible, this often requires multiple iterations to fine tune. Because of this, power consumption was not a main concern at the start of the thesis.

However, after revision of the power budget on the student satellite, the previously required power budget were reduced to such an extent that the sensor could not be supported with the projected power consumption at continuous use. The following effort went into cutting the power consumption:

Reduction of the clock speed the FPGA operated on: The main power consumer is the one doing the most work, i.e. the FPGA. This FPGA contains multiple resources in the form of hard peripherals, on chip oscillators, and both volatile and non-volatile memory. This is in addition to the FPGA fabric. Some of these resources are not in use, and most are not pushed to their limit in the form of performance. The on-chip oscillator was used to produce a 50 Mhz clock, which in turn is processed via an internal clock conditioning resource that alters the clock to the desired frequency. By lowering the desired clock frequency to 25 Mhz, the FPGA design software estimates the power consumption to now be reduced by 5 mW.

Increasing pull-up resistance for the I2C buses: Due to several I2C isolator circuits, the entire readout system had a total of 12 pull-up resistors on the bus. By using a higher resistance, less power would be consumed at the potential cost of a slower bus given a large bus capacitance. This was in turn deemed a non-solution. As the input leakage current when the bus is inactive is very low, the potential power savings would only occur during I2C transactions. For the digital-to-analog converters, these are only set up once during power on, and should have little reason to change. The temperature sensor is polled at a very slow rate as well. The main avenue to save power here would be on the external I2C lines, but as this bus uses I2C Fast, there are stricter requirements to the bus pull-up resistance. In the end, the original design using 10k Ohm resistors was kept.

In the end, the most effective power saving measure is to limit the up time of the system. To be compatible with that, the system must tolerate being shut down at any time, but also have a short boot-up time and be able to store its last configuration, so that time and energy is not wasted re-configuring the system every time it is turned on. This was achieved by using a flash based FPGA, so that the FPGA configuration image does not need to be accessed by an external memory every time, and sensor configuration in the form of digital control pin state and digital to analog converter levels are kept in a non-volatile F-RAM, which has quick access and practically unlimited write/re-write cycles. The result of this is that the system is ready to measure the sun vectors in less than 100ms after power on.

6 FPGA design

By implementing logic on FPGA and evaluating the result versus resource usage, the road map to a solution where the sensor and readout system is on one ASIC could be made shorter. This is done by either providing viable solutions, which then only requires porting over to the ASIC process, or by saving time showing that the solution is not viable, and other routes should be tried.

The FPGA is used to create custom logic with a fully deterministic behavior. As opposed to a micro controller executing commands sequentially, logic implemented in the FPGA fabric can, if designed so, operate in a truly parallel fashion. When the data bus operates as a series of interrupts, it makes sense to guarantee that all incoming data will be acknowledged without an uncertain delay. To communicate and control the sensor ASIC, an FPGA architecture was designed in which there are two duplicate lines that control each of the sensor axes. These axes operate as independent sensors, and so the FPGA's job is to record and buffer all incoming samples and time tag them, so the micro-controller can correlate and process the data.

As the sensor ASIC's two pixel lines operate as two independent sensors with their own dedicated data interfaces, the FPGA architecture has two duplicate sets of interfaces logic, time tagging and buffering, such as each pixel line can be read without affecting the other

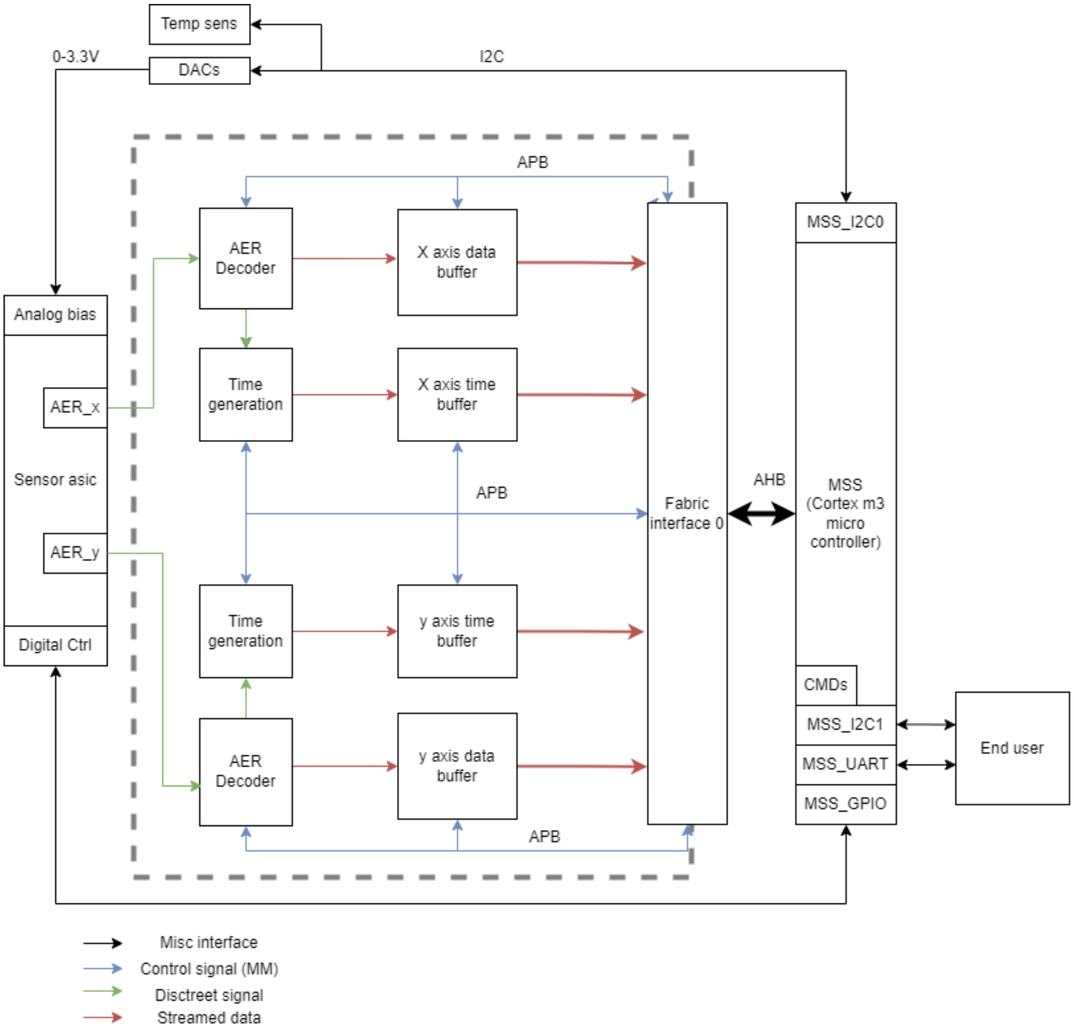

Figure 27: Architecture of the embedded system, with focus on the FPGA fabric

6.1 AER

To get data from the sensor ASIC, an AER decoder has been developed. It is used to receive the asynchronous data and present it to a synchronous system. Due to the nature of asynchronous systems, the AER decoder has a configurable number of hold cycles in which the bus has to remain stable to progress to the sampling stage. As the ASIC has a small tape-out error with the wrong polarity on the bus pin, the AER decoder instantiating has an inverter on the relevant pin. This allows the AER decoder to remain unchanged if ever implemented on another AER system.

The decoder also has the usual control interface used by the processor: enable, reset, current state, and a stepping function. The stepping function is useful in a debug situation, and works well with an asynchronous bus. When enabled, each step for the state machine is halted until the processor sets the step bit high. Then the state machine perform one step before clearing the bit. During this time the processor can readout the ports and registers.

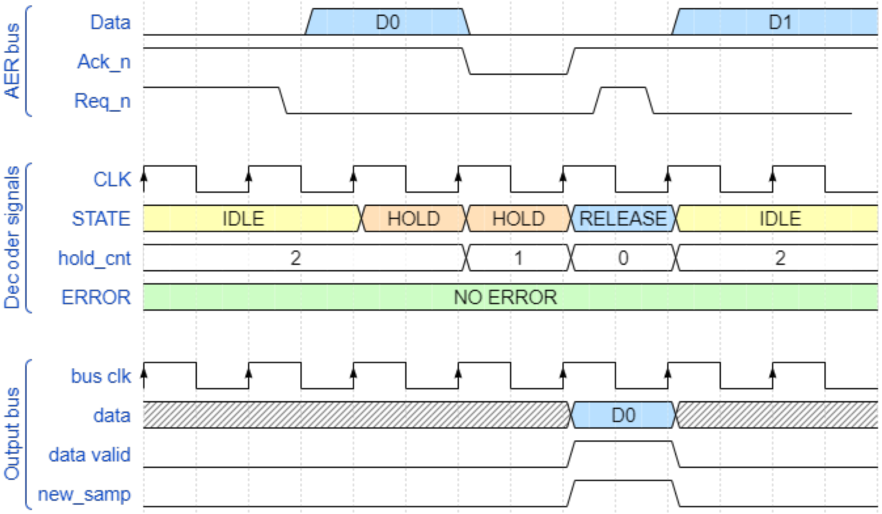

Figure 28: Waveform and timing illustration of a normal AER transaction

As can be seen in the timing diagram in figure 28, when the sensor outputs the data after the hold_cnt reaches 0, then the the data is passed to the next FPGA process.

In figure 29, the data changes during the sampling period. This triggers the hold_cnt to reset to its configurable maximum, and the unstable bus bit is set in the error register.

By setting the reset value for hold_cnt to 0, the decoder does not check for bus stability, and releases the data on the next clock cycle after it has been received.

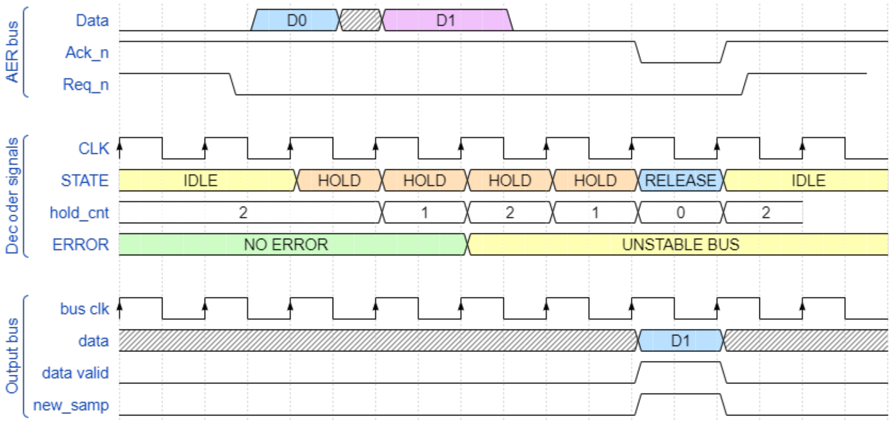

Figure 29: Waveform and timing illustration of an AER transaction where the AER bus is unstable during the hold stage

6.2 Data time-stamping

As the data or events are not generated in a fixed periodic fashion, timing information is more crucial than in typical periodic systems. Therefore each incoming event is timestamped. The system is designed to only timestamp the events after they are outputted by the decoder, not synchronized to the when the sensor outputs its data. This is to make sure that unstable bus events do not get processed into the system.

The timing generation is a straight forward clock counter that outputs its current on-time to the buffer stage once an event is outputted by the AER decoder. The time is a 32 bit counter with each step being a 20 ns step. The counter rolls over after 85 seconds.

6.3 Buffer

The system consists of 4 buffers; two data buffers and two timing buffers. The buffers are split into two pairs, with one data and one timing buffer in each pair. Data and timing buffers should always be synchronized, E.G. if 100 elements are read from the data buffer, then 100 should be read from the timing buffer. Both buffers in a pair are synchronized in its clearing. As the buffers are dual port, it can be written to while also being read from at the same time.

As the APB bus has a limited memory space for each module, it is not trivial to implement a random access type memory. As random access is not needed, a FIFO topology is the best fit for the architecture. There are two important registers the micro-controller needs to read data from the buffers; Offset 0x00 (read data) and offset 0x04 (data count).

The buffers could be realized via logic elements and flip flops, but modern FPGAs almost always have dedicated silicon structures for both memory and math functions spread over the silicon die. For the selected FPGA, there are 21 blocks with 18 Kbit SRAM structure and 22 with 1 kbit SRAM. By using these dedicated structures, logic elements are preserved for other use, and as these are highly optimized, these memory structures have a much better performance than memory realized with generic logic elements. For the buffers, 10 blocks are used per axis, where 8 are used for time tagging and 2 are used for pixel address. This means that a total of 4096 samples can be stored at a time per axis, where each sample has its own timestamp.

The buffers on one axis have their reset tied together, connected via logic or function to the global reset. This enables both buffer to be manually reset at the same time, which is required for a clean wipe.

7 Embedded Software design

The readout system runs a small embedded software written in C. The software is tasked with performing self-tests of the system, gathering meta data, presenting an external command interface to a master system and, most importantly, forwarding the data from the FPGA fabric to the master as either raw pixel addresses or processed vectors.

First the software configures the peripherals before doing a quick self test. The self test consists of polling the device ID from all attached digital circuits. Device ID is read, as it is a known constant and not a value dependent on the environment, or previous states. This test is sufficient to check for major faults where an integrated circuit is unable to do any task. This could be a typical result of a fault related to solder joints dislodging on the bus connections, or at the power supply pins. Hard shorts are not detectable, and would result in the entire readout system being inoperable.

As a part of the self test, the temperature sensor is also polled for the current temperature, the digital-to-analog converters also get their last value set, and the non-volatile memory is read for the configuration values. The sensor ASIC does not have any device ID. What it does have, is active low signals on the AER bus, which can be read after a global reset. Thus, the self-test routine part for the sensor ASIC is to set the global reset and check for the bus request signal to go high (no request).

After the configuration and self-test, the embedded software enters the operational state. In the operational state, the embedded software checks for commands on either the UART or I2C interface.

In this state the FPGA is constantly reading the incoming samples from the sensor ASIC and buffering them for the software to process. Periodically, the buffer contents are read out and cleared. Then the data is processed into a time-tagged vector, made available to the upstream master.

Data is readout by issuing commands requesting a specific amount of samples. After a readout is done, the buffers are wiped and the ASICs global reset is pulsed.

8 Mechanical design

To house the system and be able to use the system on a 1U student CubeSat, a simple aluminum frame was designed. Due to the CubeSat standard only allowing to protrude out 6.5mm[6] from the satellite glide surface, the sensor readout system and the mechanical frame needed to be as thin as possible. The maximum width of the flight model was measured to be 6.1mm.

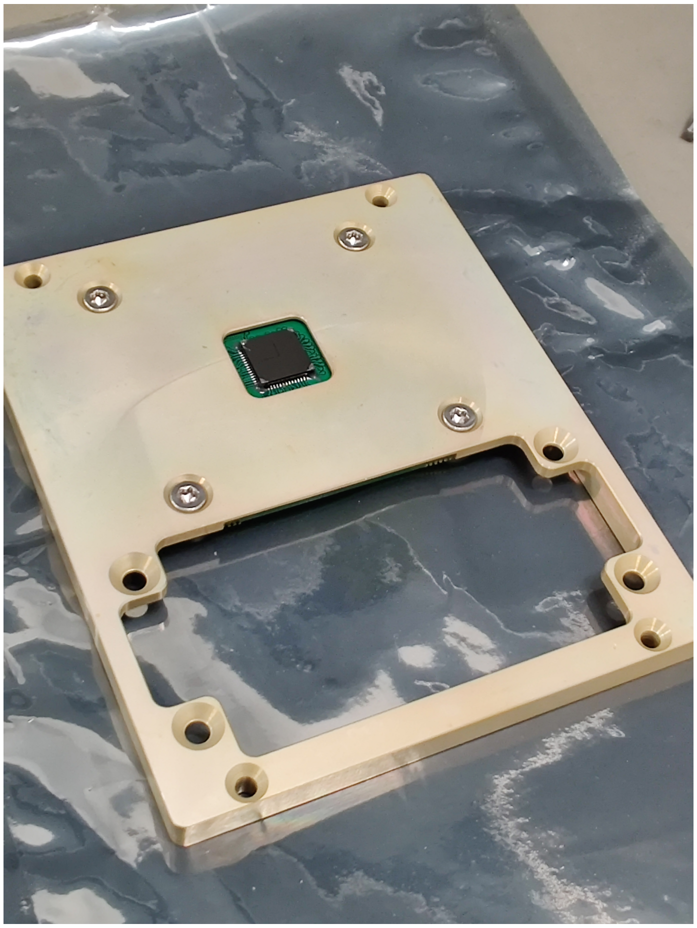

Figure 30: Photo of system inside aluminum frame, reference sensor not mounted in large hole. Optics can been seen secured with epoxy at the corners

9 Lab Tests

9.1 Functional test

Before using the system to perform tests on the sensor, the system functionality should be tested and verified. This test should also try to find any limitations or constraints that could impact the other tests planned. Other than verifying basic functions, timing and DAC accuracy should be measured. Loading of the wrongfully connected DAC outputs should also be checked.

To check that the sensor ASIC has no unexpected malfunctions before doing time consuming sweeps, the pixel array and the AER interface should be checked. To check the AER interface, two 8-bit variables for both axes, which are set at zero at start-up, is implemented. One for low-high transition, and one for high-low. Each bit is used to record that the corresponding AER data pin has transitioned. These transitions are latched in, being unable to be cleared unless reset. As the driving strength/output impedance of the AER pins are set by the Pull-up(PUx) and Pull-Down(PDx) pins, this allows for verifying that the DAC-bias voltages are working as intended. A simple flashlight can be quickly swept over the sensor to make the sensor trigger all 8 bits. If some pins have no transitions recorded, a slower sweep with more illumination should be used before concluding malfunction.

As all individual AER pins should be verified to be working and not permanently stuck, so should the pixel array. This uses a similar approach as the aforementioned test; variables in the embedded software latching in data. Two 192 long arrays are implemented, one for each axis. Each time the sensor ASIC outputs a pixel address, the corresponding address in the array is set high, making it a list of each pixel that has triggered an event. Early testing with a free-running configuration in normal room lighting has shown that two pixel neighbors often trigger right after another, followed by a jump in address.

The system should be swept on the entire FOV multiple times at small angle increments, and then the list should be read for each pass. If any pixel remains un-triggered, the scene illumination should be changed, and the steps should be reduced. The sweeping range should be reduced as well to have multiple sweeps on un-triggered pixels, before concluding with dead-pixels. Using the multiple winners mode should be allowed to compensate for some dead-pixels in that case.

To account for potential bias the readout system introduces to the sensor response, the asynchronous data bus is monitored in a test with a oscilloscope. The data here is not measured, only the sensors' *bus_req*(interrupt signal)

9.2 Lab Test Setup

The basic setup for all the tests are kept for all tests is described below:

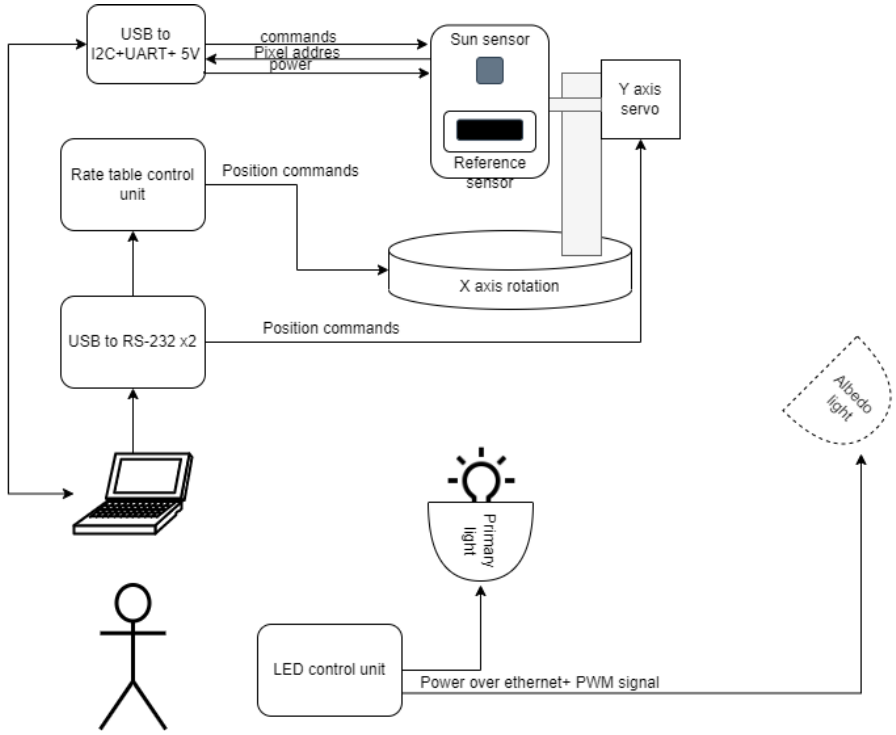

Figure 31: Illustration of the test setup

The readout system, including the reference system, is mounted on to the Y-axis servo (Animatics Smart motor SM2361DT) via a 3D printed adapter. The Y-axis servo is in turn mounted on the spin-rate table(Ideal Aerosmith 919b) via a dedicated aluminum adapter. A photo of the setup can be seen in figure 33 and figure 32

The spin-rate table provides two dsub connectors for signal pass through via the internal slip ring. This interface is only used for the Y-axis servo's electrical interface. Efforts are made to prevent the table from rotating in a half rotation in a single direction, as the readout system is interfaced via a long USB cable.

The readout system is interfaced and powered via a USB to I2C breakout board, which also features a TTL UART and a separate 5v from USB power output pin as well as a regulated 3.3V power output. This results in the entire readout system, including the reference sensor, talking to and being powered by one device, which in turn is controlled by a host PC.

The host PC controls both the X-axis (spin table) and the Y-axis (servo) via a serial RS-232 interface. A framework requesting that these actuators get into the desired positions, and polls for said actuators' status in completing the requested move, was made as scripts sending ASCII commands. This framework does not support constant motion. An additional framework was made to gather data from both the readout system and the reference sensor.

A high powered 150W LED photography lamp (GSVitec Multiled QT) was used to provide the illumination as seen in figure 34. It has a white light and provides up to 12000 Lumen. At first it seemed like the LED controller supported external control, but that option was not present for the specific model made available. This prevented having a test setup where the illumination could be finely stepped as a separate test dimension. Said lamp supports multiple optics, the 15° spread was selected as it was the most focused of the arrays of optics. The lamp was placed at the end of the room from the spin-table, which provided a distance of around 3.5 meters.

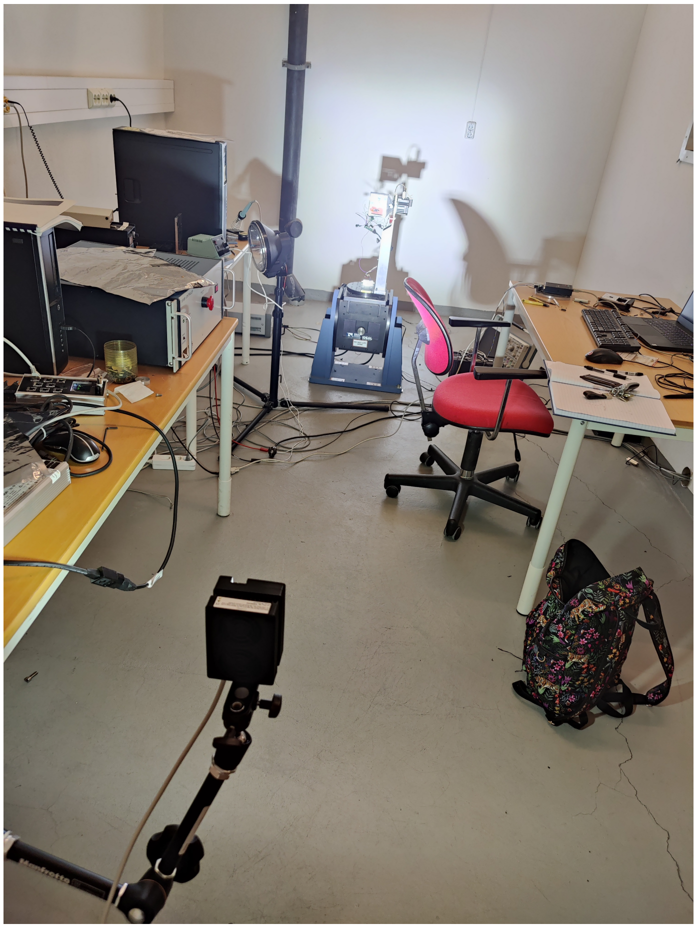

Figure 32: Photo of the test setup

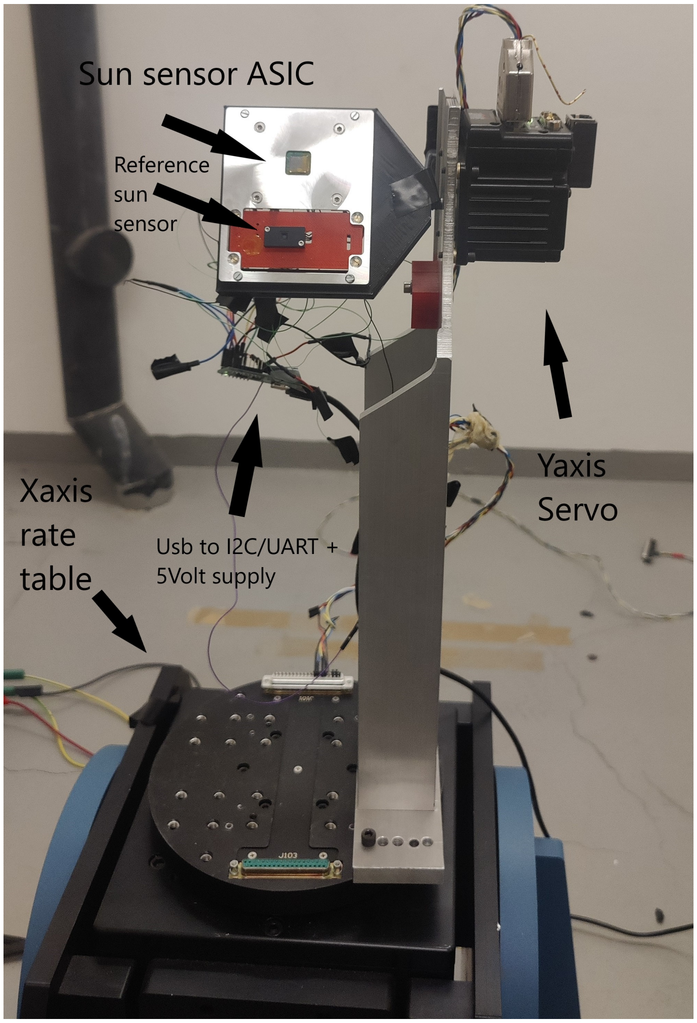

Figure 33: Close up of the readout system during test

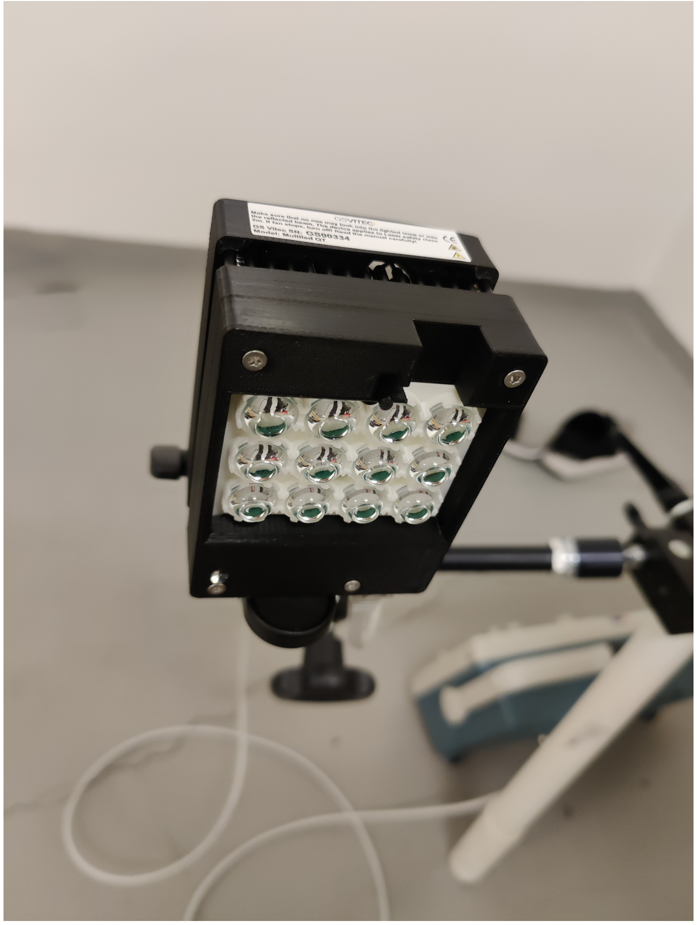
GSVITEC
Make sure that no one may look into the lighted lamp or into the reflected beam. The device applies to Laser safety class 2m. If fan stops, turn off! Read the manual carefully!
GS Vitec SN: GS00334
Model: Multiled QT
CE

Figure 34: Close up of the LED lamp used as a light source, mounted with 15° optics

9.2.1 Stepping routine

The stepping routine first moves both the spin table and the servo into the requested start position, then the spin table is stepped, while samples are taken. When the spin table has reached its end position, the servo is stepped and the spin table is moved to the starting position. Step sizes, and start and stop positions, are configured for each test.

9.2.2 Sampling routine

For all tests the sampling routine for the sun sensor and the reference sensor remains the same. Only after the position of the spin table and the servo has been confirmed via self-reporting status bits for the motor controllers, will the reference sensor take one sample, in which the raw data is stored for this particular angle. Then the sun sensor produces 250 samples 7 times, where all modes are iterated(free running, timeout, TFsN with 1,2,8 and 16 winners). The bias voltages applied to the sensor remain static during the tests. These 250 samples are stored in their respective comma separated files, where each sample is paired with the corresponding timestamp generated by the FPGA. The angle and configuration is stored as part of the file name.

9.3 Angular measurements

This subsection groups the tests related to the angular measurements. These tests aim to measure the sensor's output angle versus the rate table's angle. The difference in the tests are the region of focus. The first test, dubbed *full sweep*, consists of relatively large steps going from -60° to +60° on both axes, while the *Field of View* test starts at -80° and goes to +80° at only one axis. This test should give better insight into the sensor's characteristics in and beyond the stated FOV. The last angular measurement test is the close to center region of +-20°, with ultra fine steps on the X axis and moderately fine steps from 0° to 10° in the Y-axis. The rational to not use ultra fine steps everywhere is the very long run time such tests require. Combined with the comparatively low resolution of the sensor, ultra fine steps would not bring major benefits.

9.3.1 FOV limit

The sensor's FOV is measured by sweeping over a wider arc than the expected FOV and record the sensor response. The linearity and the error of the sensor are measured by reading out both the set position of the spin-table and a reference sun sensor. The goal is to try to determine the point where the sensor is unable to render accurate and trustworthy data.

9.4 Albedo reflection

This series of tests is performed to check the claim of immunity from the albedo effect, and gather data on the sensor's response when exposed to an emulated albedo iridescence, which in turn can be used as albedo detection. Results of this test will be used to compare how the sensor performs relative to other sensors.

9.4.1 Expectations

This is a test where it's possible to have prior expectations to the test results. By comparing the actual results to the expected response, the test setup may require some additional tuning to produce the expected response. E.g. if no albedo effect is present in the data, intensity of the albedo illumination might need to be increased, or the angle between both light sources adjusted.

The expected response for the sun sensor is to see the spread of the multiple winners increase with larger jumps in the pixel address. Some data clusters should also suddenly deviate their median value largely for samples where the albedo light is normal to the sensor

For the reference sensor, which has, to the author's knowledge, no detection or correction for the albedo effect. It is expected that the sun vector will be skewed toward the secondary light source.

9.4.2 Albedo light emulation

To be able to give these tests any weight, some effort to emulate the reflected light should first be applied to the work. The characteristics of this light are that it is diffuse, it is similar to black body radiation, it varies in intensity based on the relative location of the satellite, and it has a temporal noise stemming from the local weather.

A secondary lamp was used for this. It is of the same make as the primary lamp emulating the sun light. The optics were changed from 15° spread to the maximum 60° spread. The albedo lamp was placed much closer than the sun lamp to further amplify the scattered characteristics of the albedo light.

During the initial testing, the illumination level was set relative between the lamps instead of replicating the exact illumination (1356 W/m2 and 400W/m2 respectively.)

9.4.3 Test procedure

For this test, only the spin table is rotated. 250 samples are gathered in all configurations before stepping to the next sampling point. The sun vector from the reference sensor is also sampled before moving to the next point. The readout system is swept from -60 to + 60 in 1 degree steps, while the y axis is kept at 0. The light levels are stepped from 20% to 40% intensity between the different runs.

10 In situ tests

As a large side note, this work will try to get use of a flight opportunity. The goals for the in situ tests are as follows:

- Check that the sensor design can withstand vibration loads imposed by a rocket launch
- Measure to what degree the sun sensor is susceptible to light pollution induced by the Earth's Albedo
- Gather in situ temporal data when exposed to the sun that can be used to further refine the angular correction model.

10.1 Constraints imposed

10.1.1 Data transfer

Initially not a constraint, the satellite platform ran into some memory issues, pushing to limit the amount of data that can be gathered from the readout system.

The satellite has two ways of transferring data; periodic pings dubbed beacons, and selective file transfer. The beacons will be sent every 20 seconds and contain small amounts of data. Previous iterations of the satellite platform have much better success at transferring data without corruption with these short packets, than larger file transfers. The file transfer works by giving meta data to each file, where each file consists of a larger series of streams of raw data gathering. As there is too much data to be transferred from the satellite to the ground segment, the meta data has to be sufficient to select the most desirable files for transfer. Multiple transfers can be queued so that an operator does not need to browse all files for every pass of the satellite.

First the beacons have priority, as those have the greatest chance of delivering data. To reiterate, the goal of the in situ experiment is to gather real use performance data when compared to a typical sun sensor when placed in the same frame of reference. Multiple parts of the orbit is interesting, but it is difficult to know beforehand exactly where the satellite will point in relation to the sun on all parts of the orbit. By sending the last 4 samples in beacons, the time between them, and the corresponding reference sensor vector, after enough time the sensor should have been exposed to most possible orientations, and have had the opportunity to beacon a very low amount of data.

10.1.2 File transfer

The data stream from the sensor is decimated where the different decimation rates are applied simultaneously to different files. Meaning that data will be stored both in a high temporal resolution file and a low temporal resolution file. By first analyzing the low temporal file at the desired angle of incidence provided by the metadata for rotation rate, inaccuracy and sample spread, a decision on which high resolution files to be downloaded can be made.

The launch is highly experimental. One of the most pressing launch failures is not ending in a high enough orbit, which will result in a very short operational time for the satellite before falling back to Earth. The expected minimum orbit time is 2 months, so receiving varied comparative data between the sun sensor and the reference sensor at a large range of incidences is more desirable than receiving not varied high temporal resolution data at fewer different angles of incidence. Hence downloading the low data rate files first is the priority.

By pairing the data from the sun sensor and the reference sensor with data from the onboard magnetometer, the relationship between the Earth and the satellite can be established.

11 Results

This section will showcase and describe the results from the previous tests performed.

11.1 Angular data

Figure 35 shows the raw response of the sensor when only the most illuminated pixel is allowed to output its address from -50 to +50 degrees. This measurement gives the basis for setting two of the major calibration values: the middle pixel value and height adjustment. Ideally the middle pixel should be 96, but 76 seems correct from the raw data. Focal distance, the distance between the sensor pixels and the optics, is assumed to be correct from [4] at $356\mu m$. The first level of calibration to convert pixel address to angle of incidence for this assembly of the sensor then can be filled in equation (3)

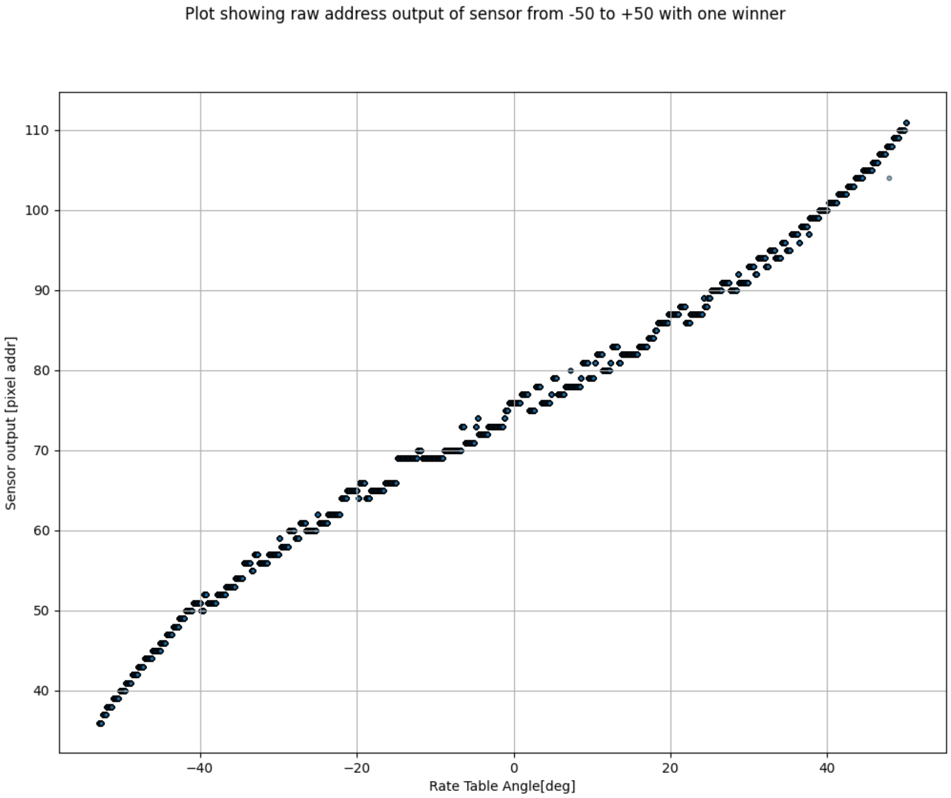

Figure 35: Plot showing the raw output of the sensor in winner takes all mode (default)

Figure 36 shows the sensor response when calibrated with pixel 76 at center pixel. Key information is that the output angle exhibits a linear behavior, and matches the rate table's position at -40, -20, 0, 20 and 40 degrees. Notice that the accuracy is much better outside the +/- 20 degree region, as claimed in section 3.3.

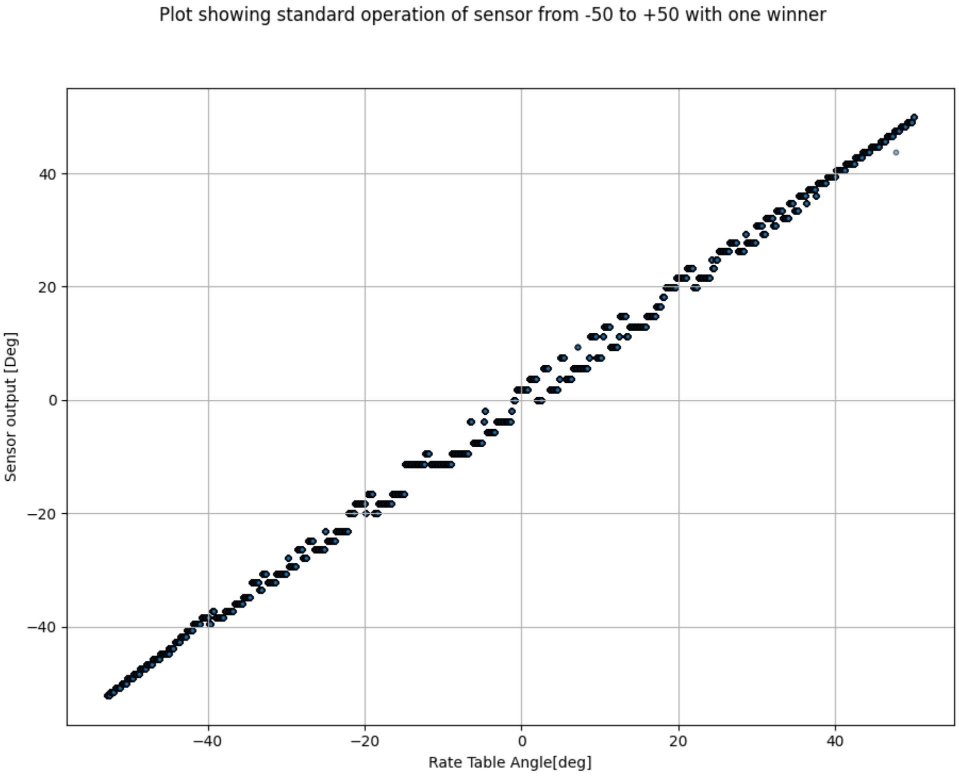

Figure 36: Plot showing normal sensor response in one winner takes all mode

11.2 Temporal data

The goal of using temporal data is to check if the worse case regions' accuracy can be improved. Figure 37, shows the accuracy in the latency vs the variance seen in the sensor output. The top plot shows the time it takes the sensor to produce and transfer one 8 sample cluster to the FPGA. The bottom plot shows the median angle from all samples in a cluster. There are around 12 clusters for each measured point, which is stepped 0.1°. The main takeaway from this plot is that the sensor's output angle has a large even variance while the latency follows a distinct pattern where the latency is at one of three points at each measurement point; very fast, follows a rising pattern, or follows a sinking patterned which is shifted upwards. Even if the latency is scattered between these points, cluster delays for the same point has very little variance, as seen in figure 38. As the plot is a scatter plot with slightly transparent dots, the darker the color the more occurrences are happening on that point.

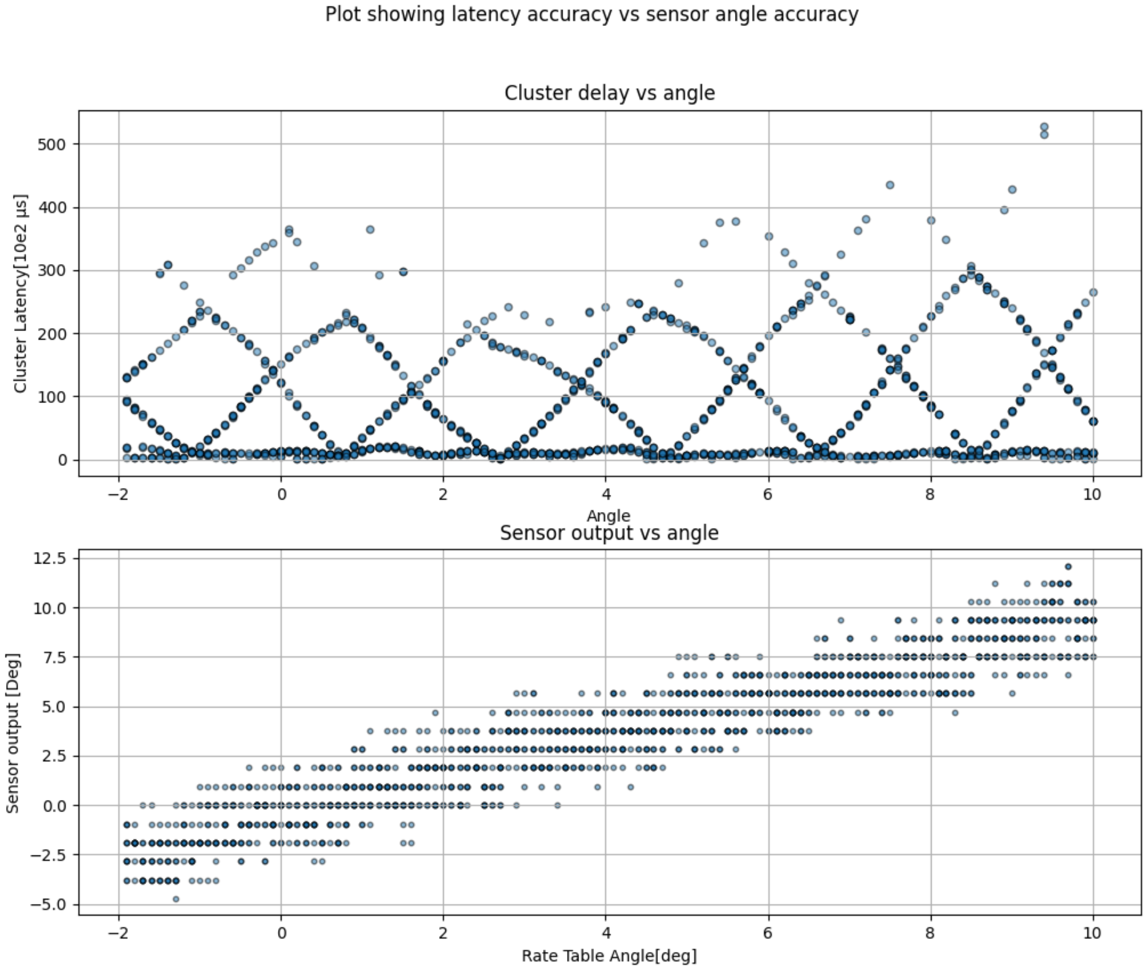

Figure 37: Delay per cluster versus angle. Sensor angular data included

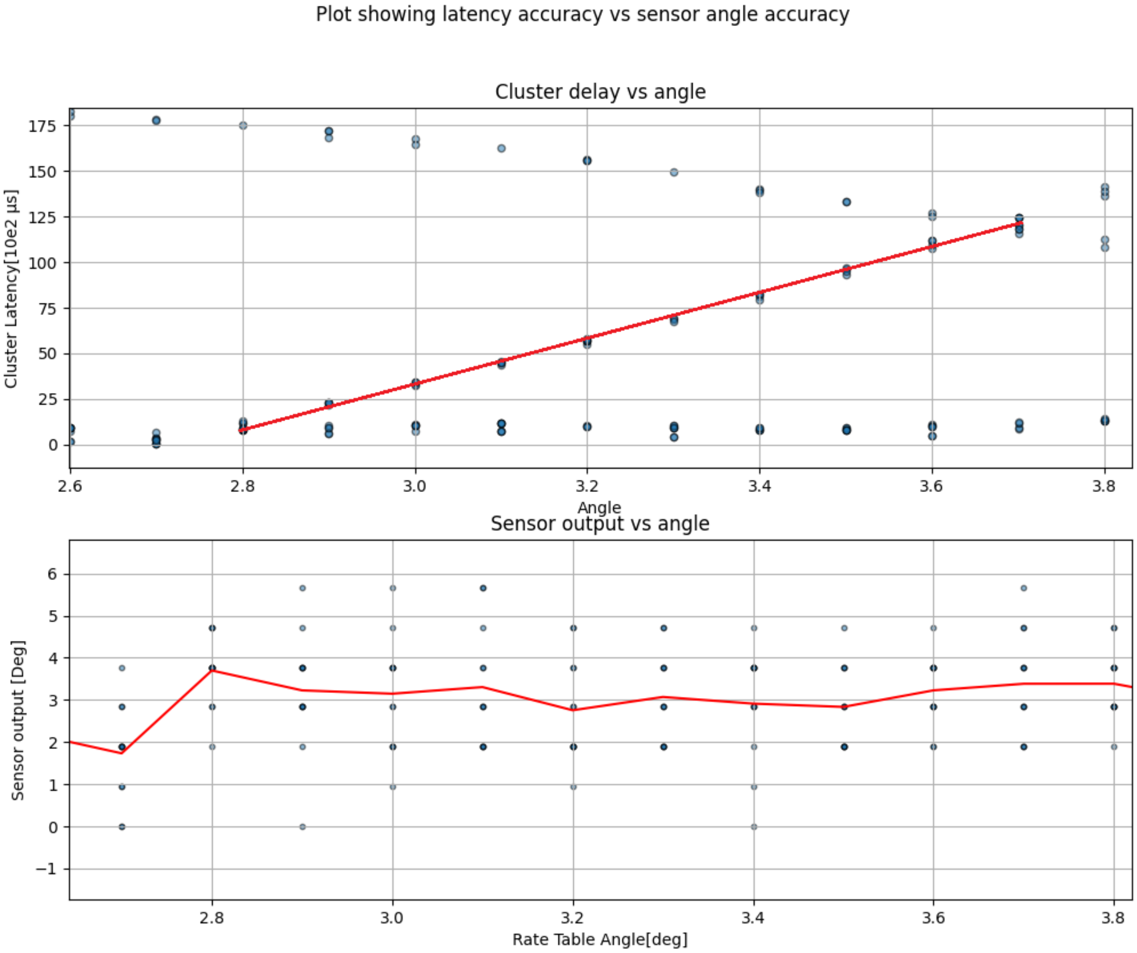

Figure 38: Zoomed view showing the latency trend line drawn from the minimum latency to the maximum, where the neighboring pixel is now the most illuminated. Bottom plot has trend line on cluster median angle, showing a non linear behavior staying around the same angle for 1 whole angle of incidence

The original measurements were on single samples, and not clusters in themselves. That distinction leads to two differences in the results. The latency has been changed by a magnitude, as the time for 8 pixels being triggered is significantly larger than for just one. It is wrong to assume that since best case for just one pixel is at 88 μS, that 8 would just take 8 times as long. The most illuminated takes 88 μs, the second most illuminated will by definition take more than this time, and so on, until we get to the last sample in the cluster.

In figure 38, we see a zoomed in version of figure 37 showing the rising latency for one pixel, which is in full view when the angle of incidence is approximately 2.7°. Said latency rises until the angle of incidence is at 3.7°, where the pixel which is in full view at 4.7°(shown in figure 37) start to take over the role as the most illuminated pixel. The top view has a manually added trend line for the cluster samples relevant to the rising pattern, and the bottom view has a line showing the mean value of all clusters median value for that given point.

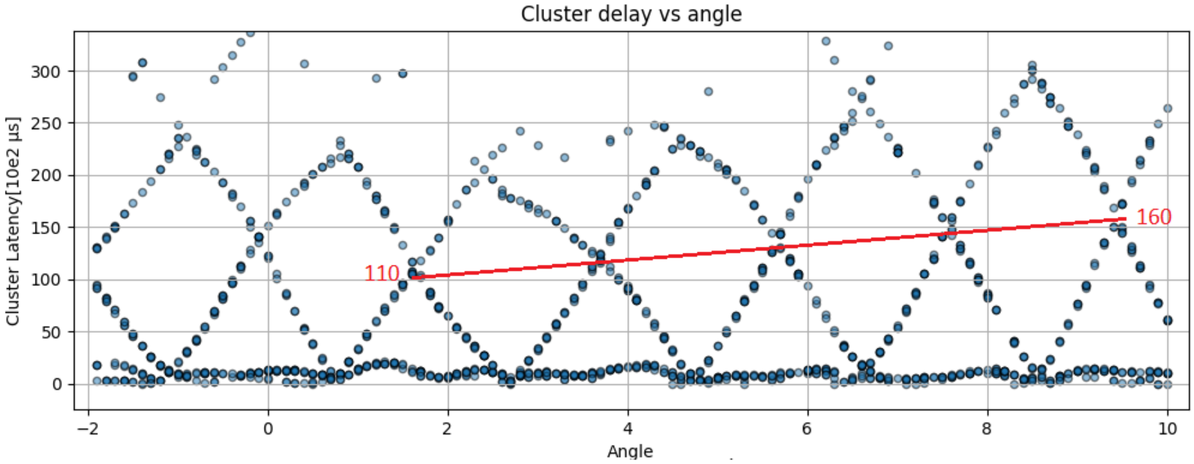

Figure 39: Cluster latency plot, showing trend of maximum pixel delay in pattern.

Figure 39 shows the increased latency the further the angle of incidence is increased. This trend seems to follow a linear rise from 1100 us to 1600 us.

11.2.1 Using the temporal data

Based on these result, an example (figure 40) can be made of how the temporal data can be transformed into the desired triangle wave. First, all values over the characterized cross point have their value over the cross point inverted. Then, all points below a lower cutoff point are removed. Then the median for the samples is calculated and can from there be used as a calibration point. Fitting based on figure 39 is used, but the folding of the top pattern is unsuccessful when the top pattern is not linear, as can been seen at around the 2.5° point, at which the median gets a peak in the wrong direction.

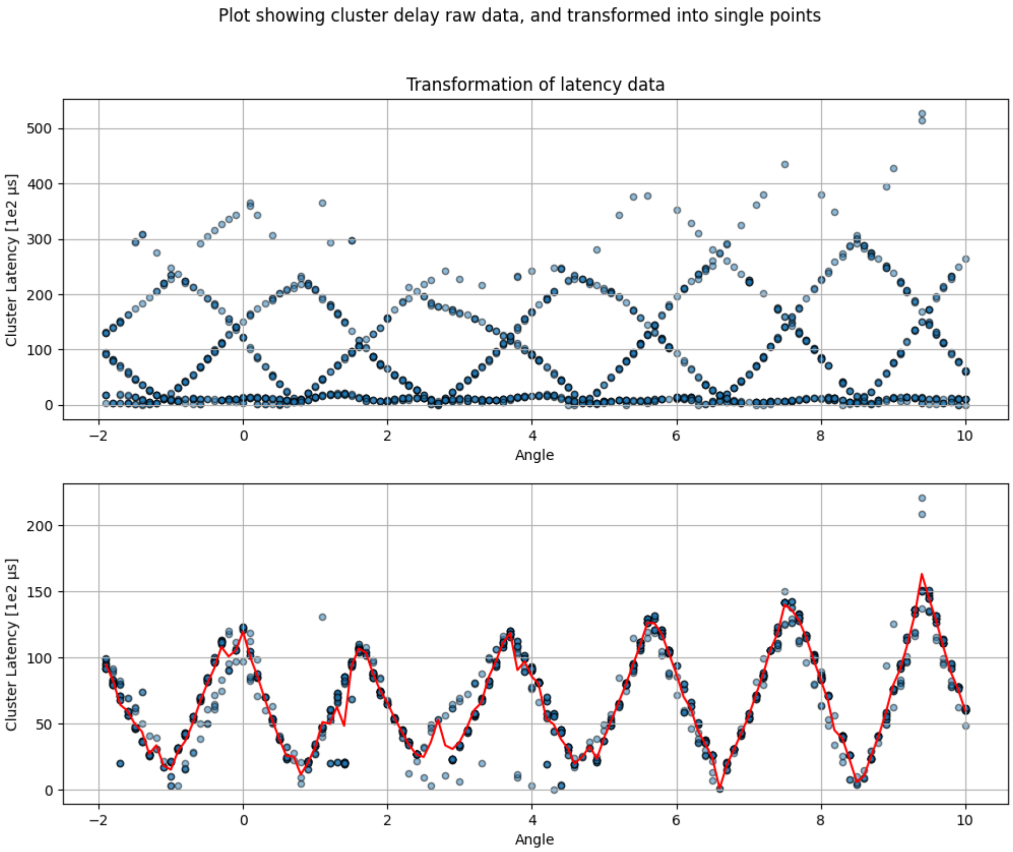

Figure 40: Plot showing how the output data would be if based on temporal data

Unfortunately, due to the fact that the sensor can output the same pixel for multiple angles of incidence interlaced between other pixel outputs as seen in figure 41, correction for the entire near region is not feasible in a trivial manner.

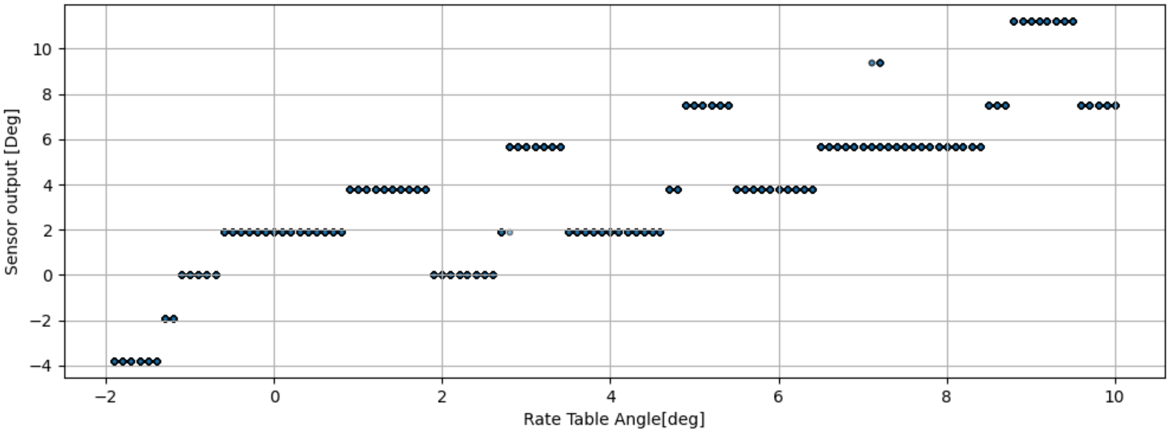

Figure 41: Plot showing the most active pixel in the near center region. The same output is given for multiple different incidence angles

11.3 Field of view test result

The results from the field of view test are quite conclusive. Figure 42 shows the pixel with most occurrences plotted from -79° to +80°. Plotting the pixel with most occurrences for each sample point is in reality just a very strict low-pass filter.

The sensor fails to track the rotation from the rate table slightly differently on the different ends of the sampling. At +77°, the sensor starts to output the same value as at +76°, then at 78° the sensor fails to detect anymore light from the lamp, and outputs -13°, most likely a result of the room reflection. For -68°, the sensor does not repeat the same address for multiple rate table angles, but has two *out of FOV* values, first -59°, then -13°, pointing to not the reflection of the room but rather a single pixel being much more sensitive than the others in a very low light situation.

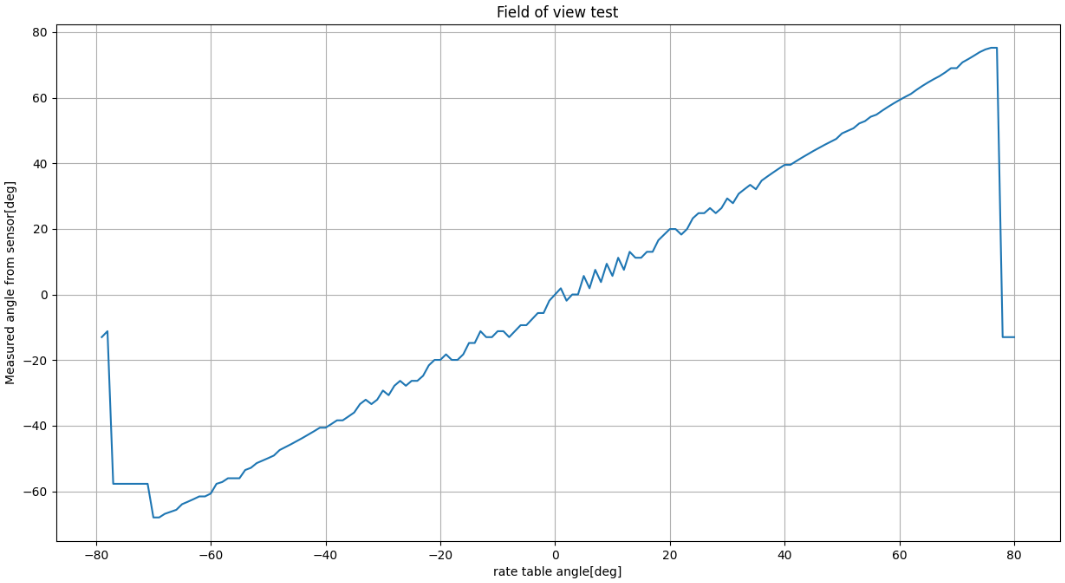

Figure 42: Plot showing the results for the field of view test, drop of is at x = -68° and +76°

11.4 Albedo test results

The albedo tests are somewhat inconclusive as when processed, the test setup fails to induce any major effect on either the sun sensor nor the reference sensor for the applied light levels. The only data to point to susceptibility is 4 clusters at -30°, as seen in figure 43. The reference sensor (seen as the red line), does not show the expected dip around -30°, but a closer inspection shows a slight shift, as it is never able to output 0, and generally is higher than it should be until it reaches 25°, where the secondary light falls out of FOV. At that point the reference sensor is able to produce a more correct value. In short, only a slight susceptibility is seen in both the reference sensor and the sun sensor. Error at the edge of field of view is surprisingly good, at 1° error at -68° and an error of 0.8° at +76 without further calibration. Better alignment of optics and silicon die could make the FOV more symmetric. The end FOV is then 144°, which is in accordance with findings in [4].

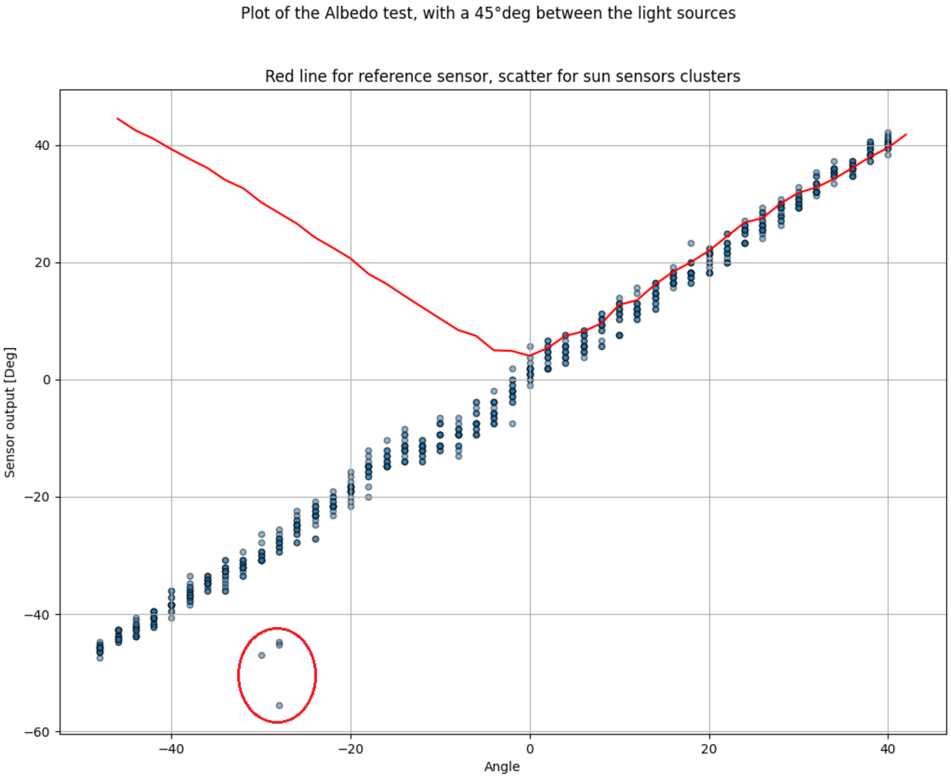

Figure 43: Plot showing the sun sensor and the references sensor's absolute output when exposed to 2 light sources at 45 degrees with the primary lamp being at 100% and the secondary at 40% output power. Minor susceptibility marked with circle

12 Discussion

12.1 Issues

This subsection will briefly list the issues found during the work on the sensor ASIC, as well as issues with the work.

Some ASICs had broken or bent bonding wire. Some wires either touched each other or the ground plane, resulting in shorts. The exact specimen used for the test only had one working axis, which hampered much of the original scope of the test. The last fully working ASIC specimen was sent earlier to be integrated in the student satellite.

The batch of lids has a varying width of the slits in from the lithography process. [4] lists a varying set of dimensions on the slit, from 50um to 160 um. Variance seems larger. The smallest ones are used in hope of better accuracy. This might have been the incorrect call. Future testing should include both ends of the width spectrum to investigate the trade offs for the slit width

TfnS mode promises in its description in [4] that each pixel will only trigger once until a reset is given. Evaluation of the raw data has shown that there are several occurrences of the same pixel address being outputted in sequence within one cluster and reset cycle. This could be the result of insufficiently tuned bias for the pull up and pull down transistors.

Preparation and adaption for the in situ tests was a time consuming task which could have been better spent on matters more related to lab tests in this work.

12.2 Discussion on the results and the work

12.2.1 The need for calibration

Tests performed prior to calibration of the sensor shows the need for the calibration. As one cannot visually check for the correct alignment between the silicon die and the optics, the center pixels needs to be found via characterization. The conversion from pixel address to sun vectors require several operations, but could be implemented as a calibrated look-up table with an output angle for each of the 192 pixels.

12.2.2 The readout PCBs

The overall electrical design was done quickly over 2 weeks, and was primarily driven by the need to deliver a working sensor and readout system for the student satellite. The satellite was also the main design driving factor, which set budgets on power and form factor. A readout system designed primarily for testing would be better for this work. A socket container for the sensor ASIC would, for example, give the ability to test multiple ASICs on the same platform, reducing the potential impact on batch variance on DACs. In all, the electrical design was made flexible enough to accommodate what was needed.

12.2.3 The testing

Testing was done with a focus on easily available equipment. The light source was the brightest lamp that was not spoken for, but not a true sun simulator. As such, the results of the test might vary when performed with a different light source with a different light spectra, but they should not vary to a degree where the findings would be nullified.

Testing was performed with keeping one axis static while changing the other instead of varying both at the same time. Where the fine control of both axes was important to characterize the sensor in [1], in this work, as the different sensor axes work as independent sensors, this is less important, and was therefore not prioritized. this was deemed an acceptable in order to be able to finish the work in the given time.

All tests have been performed in ambient temperature. Temperature often has a negative impact on the repeatability for measurements performed with imaging sensors, mostly due to dark currents. The sun sensor does not have any temperature compensation, and this is out of the scope of this work. Regardless of this fact, it does not seem that variance in temperature from a cold start at ambient temperature up to the peak temperature of the sensor, which should occur when the sensor is normal to the light source, introduces any sudden inexplicable characteristics.

12.2.4 Light source

In hindsight, using LED lamps could be an issue due to the intensity controller. It is most likely realized as a simple pulse width modulated signal, where the duty cycle is directly linked to the desired light level. If the base frequency is too low, it could be possible to pick up the variance in the light level if the sensor is fast enough. As it stands, there is no definitive evidence that using the LED lamps in their pulse width modulation mode has affected the measurements.

Unlike tests performed in [1], the parallelity of the light was not controlled, but assumed to be acceptable. The optics of the lamp gave a view angle of 15°, while the view angle of sun light is closer to 0.5°. This in combination with the lamp design consisting of not one light source, but an array of 3x4 LEDs, the sun sensor is exposed to potentially non representative light environment which could result in the larger spread in angular data. A collimator could be used to achieve a more representative view angle for the light.

12.2.5 Albedo testing

A larger and more desired effect on the reference sensor due to the secondary light source has been observed in earlier testing, but was not recreated in the last round of tests. This is most likely due to the optics used on the lamp. Originally 15° optics was used on both lamps, but for the last set of tests performed, the albedo lamp was changed to 60° to better emulate the more diffuse light albedo reflection is. The lacking expected susceptibility was not found out in time to redo the tests with a setup being able to affect the reference sensor to the desired level.

Even so, there were a few clusters pointing to some susceptibility, which points to the test setup not being entirely useless. However, it is difficult to use it as a good basis to make a claim on albedo immunity. As it currently stands, there is a combination of angles of incidence from multiple sources with different intensity that triggers some samples to contain erroneous values, even if the amount of samples are low.

Cluster spread is typically within +/-7 degrees on the worst case angles of incidence, and at around 3 at the more ideal angles. Getting a sudden cluster which falls outside this spread should be discarded to provide albedo protection. This is as long as there is a vast difference in the quantity of *non albedo clusters* compared to the affected samples.

Due to the varying nature of reflection of the Earth based on the albedo, the test measuring susceptibility is not adequate to recreate the irradiance environment. Better performance at this scenario suggests less susceptibility in real life, but the test does not act as any guarantee of correct behavior. Hence these tests should be performed in a comparative way, with multiple types of sun sensors exposed to non-ideal light pollution to gain confidence in a sensor's actual performance.

12.2.6 The sensor ASIC

One unexplored advantage over other types of sun sensors this sensor potential could have is longevity. Photo-diodes exposed to irradiation will have a degraded output current over time. This affects all sun sensors, as the photo diodes are not hidden behind an aperture. For a traditional analog 4 diode sensor, an asymmetric degradation will quickly render the output of the sensor less trustworthy, as the ratio of the diode output gives the angle of incidence. As this sun sensor can output a vector based on the median photo-diode from a series, the ratio between these matters much less, assuming that the same pixels trigger but in a different order than on a non-degraded platform.

12.2.7 Temporal data and findings

This work has gone through several iterations of what in fact should be the main focus. In the end, the point of interest was found in figure 21. The pattern of the latency hidden in the random points were alluring, and matched what I myself understood of the sensor's behavior. As these data were not discussed in detail, nor repeated in any other of the many tests performed in [4], paired with the fact that the region of operation which had the worst resolution also featured the latency pattern, it seemed like an interesting effect to investigate.

By evaluating the latency between clusters, much of the randomness of the latency is evened out. The latency pattern is not identical to the shape seen in figure 21; there are two shapes moving in opposite directions, and a lower line of relatively equal latency. When going through the raw data it can be seen that a cluster with a long inter cluster latency is often, or always, followed by a cluster with a short delay. The best way to use this data is to simply check for two levels instead of just one.

Based on the findings it should be possible to implement data processing that provides angular correction based on the latency between sample clusters, as the behavior is very linear. The main challenge is getting angular data that is unambiguously in a given range of angles of incidence. Measurements taken have some other pixels interleaved with the most illuminated pixel. Using multiple winners instead of just the most illuminated pixel, could help, but the same problem persists.

Latency should be adjusted for tilt in the other axis, so that when data on one axis is present, the previous (un-corrected) data from the other axis should be used to create an offset to the expected latency pattern. Then when the other axis has triggered, the raw data from the first axis should in turn be used for the latency offset.

12.3 Future work

12.3.1 ASIC

A larger sample of sensor ASICs should be tested to validate the characterization data, and to better describe the production variance inter and intra batch. Different optics should be considered as well, including the use of micro lenses on each pixel.

The current iteration of the sensor lacks the ability to make threshold and gain adjustments to pixels on an individual level. This is a feature that is commonly available on traditional imaging sensors. The lack of this feature greatly reduces the calibration ability, and as a result it would in turn require stricter tolerances for the fabrication process to make a consistent sensor.

The inside of the optics should not be reflective, as the die itself is inherently reflective. By making the inside of the optics absorb the reflected light from the die, potential false triggers could be limited. Part of this is already acknowledged by applying a non-reflective coating on the silicon die, but when exposed to direct sunlight in a space environment, the coating might not be sufficient, and the reflectivity of the optics has no benefits.

12.3.2 Data processing and management

The sun sensor has to be managed and controlled dynamically in order to be able to get the most use out of it. The actual use of the sensor should be taken into consideration when implementing management, as quick rotation limits both the use of multiple winners mode and the proposed angular correction via temporal data. Future work should investigate at which point the rotation introduces more noise than just receiving the most active pixel.

it was seen during testing, that using a high count in multiple winners mode close to the end of field of view actually decreases the accuracy instead of increasing it. The region near the end of the FOV is where the sensor has its best resolution, and therefore it only using the single winner takes all mode should be sufficient. Thus, the ideal management of the sensor dynamically changes between the different modes to try to get the best of both worlds; increased resolution in the near center region, and increased noise immunity in the end of FOV region. Mode could be determined based on last samples angle, or all modes could be used in succession as done in the tests performed in this work.

13 Summary and Conclusion

This work has revolved around characterization of an event based sun sensor, where pixel latency is measured with a readout system in addition to the angular output data. Said readout system for the sun sensor has been implemented on a stacked PCB system using an FPGA. This system has been used in lab tests for sensor, and will also be used in situ on a student satellite.

The angular performance of the sensor is worst near the center view, and improves the further towards the end of field of view. While the angular data has a worst case resolution of 1.88°, the readout system was able to measure linear changes in the pixel event latency at 0.1°. Using this latency data to increase the resolution and accuracy for the angular data is proposed, while attempts as performing this failed in this work.

The sensor's field of view was measured to be larger than reported, from 144 to 154° (77° from center). performance in this region is poor until angle of incidence is less than 65°.

The sensor has been exposed to multiple simulation light sources to check for albedo reflection behavior, in which the sensor has shown some minor susceptibility, but tests should be performed again with other light configurations.

At the current design iteration of the sensor, it provides both acceptable performance without too many requirements imposed on the end user, but there is still much room for improvement, and the asynchronous nature of the sensor should be leveraged instead of discarded. If this is done, the potential accuracy boost could make the sensor highly desirable.

List of references

[1] David Bang. “A Sun Sensor for the CubeSTAR Nano Satellite”. PhD thesis. Oslo: University of Oslo, 2013. URL: http://urn.nb.no/URN:NBN:no-38638.

[2] Dan D. V Bhanderi. “Spacecraft attitude determination with earth albedo corretted sun sensor measurements”. OCLC: 475155348. PhD thesis. Aalborg: Department of Control Engineering, Aalborg University, 2005.

[3] *Every Satellite Orbiting Earth and Who Owns Them — Dewesoft*. URL: https://dewesoft.com/daq/every-satellite-orbiting-earth-and-who-owns-them (visited on 03/26/2023).

[4] Łukasz Farian. “Biologically Inspired Sensors for Attitude Determination and Color Processing”. PhD thesis. University of Oslo, 2019.

[5] Phillip Häfliger. *CAVIAR Hardware Interface Standards, Version 2.01*. 2004.

[6] Alicia Johnstone. *CubeSat Design Specification*. California Polytechnic State University, Feb. 2022. URL: https://static1.squarespace.com/static/5418c831e4b0fa4ecac1bacd/t/62193b7fc9e72e0053f00910/1645820809779/CDS+REV14_1+2022-02-09.pdf (visited on 03/08/2023).

[7] Greg Kopp and Judith L. Lean. “A new, lower value of total solar irradiance: Evidence and climate significance”. In: *Geophysical Research Letters* 38.1 (2011). ISSN: 1944-8007. DOI: 10.1029/2010GL045777. URL: https://onlinelibrary.wiley.com/doi/abs/10.1029/2010GL045777 (visited on 02/16/2023).

[8] Klaus Mangold, Joseph Shaw, and Michael Vollmer. “The physics of near-infrared photography”. In: *European Journal of Physics* 34 (Nov. 1, 2013), p. 51. DOI: 10.1088/0143-0807/34/6/S51.

[9] Grant Matthews. “Celestial body irradiance determination from an underfilled satellite radiometer: application to albedo and thermal emission measurements of the Moon using CERES”. In: *Applied Optics* 47.27 (Sept. 20, 2008), p. 4981. ISSN: 0003-6935, 1539-4522. DOI: 10.1364/AO.47.004981. URL: https://opg.optica.org/abstract.cfm?URI=ao-47-27-4981 (visited on 03/30/2023).

[10] Alex Ryer. *Light measurement handbook*. OCLC: 659505573. Newburyport, MA: International Light, 1997. ISBN: 9780965835695.

[11] Marcel J. Sidi. *Spacecraft Dynamics and Control: A Practical Engineering Approach*. 1st ed. Cambridge University Press, Feb. 13, 1997. ISBN: 9780521550727 9780521787802 9780511815652. DOI: 10.1017/CBO9780511815652. URL: https://www.cambridge.org/core/product/identifier/9780511815652/type/book (visited on 03/26/2023).

[12] W. Wu, Y. Liu, and G. Wen. *Spectral solar irradiance and its entropic effect on Earth's climate*. preprint. Earth system change: climate prediction, Jan. 25, 2011. DOI: 10.5194/esdd-2-45-2011. URL: https://esd.copernicus.org/preprints/2/45/2011/ (visited on 03/31/2023).

[13] Ning Xie et al. "A CMOS Image Sensor with row and column profiling means". In: Nov. 2008, pp. 1356–1359. DOI: 10.1109/ICSENS.2008.4716697.